doi:10.1016/j.jmb.2008.05.017 J. Mol. Biol. (2008) 380, 386–403

JMB

Available online at www.sciencedirect.com

ScienceDirect

ELSEVIER

Molecular Structure and Metal-binding Properties of the Periplasmic CopK Protein Expressed in *Cupriavidus metallidurans* CH34 During Copper Challenge

Beate Bersch[1]*, Adrien Favier[1], Paul Schanda[1], Sébastien van Aelst[2], Tatiana Vallaeys[3], Jacques Covès[1], Max Mergeay[2] and Ruddy Wattiez[4]

[1]*Institut de Biologie Structurale Jean-Pierre Ebel, UMR5075, Commissariat à l'Energie Atomique, Centre National de la Recherche Scientifique, Université Joseph Fourier, F-38027 Grenoble, France*

[2]*Molecular and Cellular Biology, Belgian Center for Nuclear Energy, SCK•CEN B-2400-Mol, Belgium*

[3]*UMR782 Génie et Microbiologie des Procédés Alimentaires, Institut National de la Recherche Agronomique, AgroParisTech, F-78850 Thiverval-Grignon, France*

[4]*Département de Protéomique et de Biochimie des Protéines, Université de Mons-Hainaut, B-7000 Mons, Belgium*

Received 20 February 2008; received in revised form 6 May 2008; accepted 8 May 2008
Available online 15 May 2008

Edited by M. F. Summers

The *copK* gene is localized on the pMOL30 plasmid of *Cupriavidus metallidurans* CH34 within the complex *cop* cluster of genes, for which 21 genes have been identified. The expression of the corresponding periplasmic CopK protein is strongly upregulated in the presence of copper, leading to a high periplasmic accumulation. The structure and metal-binding properties of CopK were investigated by NMR and mass spectrometry. The protein is dimeric in the apo state with a dissociation constant in the range of 10^{-5} M estimated from analytical ultracentrifugation. Mass spectrometry revealed that CopK has two high-affinity Cu(I)-binding sites per monomer with different Cu(I) affinities. Binding of Cu(II) was observed but appeared to be non-specific. The solution structure of apo-CopK revealed an all-β fold formed of two β-sheets in perpendicular orientation with an unstructured C-terminal tail. The dimer interface is formed by the surface of the C-terminal β-sheet. Binding of the first Cu(I)-ion induces a major structural modification involving dissociation of the dimeric apo-protein. Backbone chemical shifts determined for the 1Cu(I)-bound form confirm the conservation of the N-terminal β-sheet, while the last strand of the C-terminal sheet appears in slow conformational exchange. We hypothesize that the partial disruption of the C-terminal β-sheet is related to dimer dissociation. NH-exchange data acquired on the apo-protein are consistent with a lower thermodynamic stability of the C-terminal sheet. CopK contains seven methionine residues, five of which appear highly conserved. Chemical shift data suggest implication of two or three methionines (Met54, Met38, Met28) in the first Cu(I) site. Addition of a second Cu(I) ion further increases protein plasticity. Comparison of the structural and metal-binding properties of CopK with other periplasmic copper-binding proteins reveals two conserved features within these functionally related proteins: the all-β fold and the methionine-rich Cu(I)-binding site.

Keywords: copper chaperone; heavy-metal resistance; Cu(I); NMR; mass spectrometry

*Corresponding author. E-mail address: beate.bersch@ibs.fr.
Present address: P. Schanda, Physical Chemistry, ETH Zürich, CH-8093 Zürich, Switzerland.

Abbreviations used: C12E5, pentaethyleneglyco monododecyl ether; ESI-MS, electrospray ionization mass spectrometry; H/D exchange, hydrogen/deuterium exchange; hetNOE, $\{^1H\}^{15}N$-heteronuclear NOE; HMQC, heteronuclear multiquantum coherence; HSQC, heteronuclear single quantum coherence; NOE, nuclear Overhauser effect; NOESY, NOE spectrometry; RDC, residual dipolar couplings; TOCSY, total correlated spectroscopy; XAS, X-ray absorption spectroscopy; ESI-MS, electrospray ionization mass spectrometry.

Introduction

Copper is required by all living organisms as a redox-active cofactor for vital processes such as electron transport, free radical detoxification, and respiration.[1,2] An essential element of numerous enzymes, copper can nevertheless damage cells by catalyzing the production of free radical species.[3] Therefore, several mechanisms exist in cells to maintain a suitable level of intracellular copper and control its oxidation state. In humans, copper imbalance is a key factor in the etiology and pathology of numerous neurodegenerative diseases, such as Menkes, Wilson's, Alzheimer's and Parkinson's diseases,[1,4,5] and both copper deficiency and excess produce adverse health effects. On the other hand, huge quantities of copper are regularly released in the environment by anthropogenic processes, and soil microorganisms are the first to be subjected to metal contamination. Therefore, understanding copper resistance in bacteria is essential for the characterization of the bioavailability and the fate of copper compounds in the environment.

Numerous cases of acquired resistance to copper have been reported in bacteria. Copper-resistance genes are often located on plasmids, as opposed to the chromosomal genes involved in copper homeostasis.[6–9] Acquired and transferable copper resistance has been studied in gamma-Proteobacteria such as *Escherichia coli*[7,9,10] and *Pseudomonas syringae* and *Pseudomonas putida*,[11,12] as well as in the Firmicute *Enterococcus hirae*.[13] In *P. syringae* pv. *tomato*, the *copABCD* operon encodes the structural resistance genes, and is transcribed from a copper-inducible promoter controlled by the two-component regulatory module *copRS*.[14] In *E. coli*, a similar plasmid-borne *pcoABCD pcoSR pcoE* locus is involved in Cu(II)/Cu(I) handling, containing an additional gene *pcoE* regulated by a separate copper-regulated promoter.[7,10]

Cupriavidus metallidurans CH34,[15] formerly *Alcaligenes eutrophus*, *Ralstonia eutropha* and *Ralstonia metallidurans*,[16–18] is a beta-Proteobacterium which thrives in the presence of millimolar concentration of multiple heavy-metals (Cu(II), Zn(II), Cd(II), Co(II), Pb(II), Hg(II), Ni(II), and Cr(VI)), and represents an important model to study resistance to heavy metals.[16,19–21] The genome of *C. metallidurans* CH34 contains two large plasmids pMOL28 (164 open reading frames, 171,459 bp) and pMOL30 (250 open reading frames, 233,720 bp) carrying gene clusters that encode machinery for resistance to various heavy metals.[22] Recent transcriptomic and genomic studies have shown that genes involved in the resistance to Co(II), Cr(VI), Hg(II) and Ni(II) are located within a genomic island on pMOL28 . The resistance to Cd(II), Co(II), Cu(II), Hg(II), Pb(II) and Zn(II) involves genes concentrated within two genomic islands on pMOL30.[22,23]

Copper resistance of *C. metallidurans* CH34 involves efflux/resistance mechanisms required for cytoplasmic and periplasmic detoxification. In this context, microarray analysis shows that the *cop* determinant of pMOL30 involves a large number of genes compared to *E. coli* and *P. syringae*.[22,23] The 21 *cop* genes that are highly upregulated by Cu(II) are named *copVTMKNSRABCDIJGFOLQHEW* and comprise the basic *copSRABCD* operon as well as *copF*, encoding the CopF P1-ATPase mediating the detoxification of the cytoplasm.[20,24] Moreover, the pMOL30 copper response cluster probably includes some other genes, such as the gtr_2 and *sil*CBA genes (a tricomponent cation–proton–antiporter efflux system).[23] On the basis of the similarity of their sequences to other systems, the CopSRABCD and CopF proteins are expected to participate in basic mechanisms for removal of copper from the cell. The function of the other pMOL30 Cop proteins, however, remains unclear. Yet it is thought that all these proteins are required to ensure an appropriate response to high concentrations of Cu(II), as found in industrial biotopes highly polluted by heavy metals and to which most bacteria equipped with *cop*/*pcoABCDRS* genes could not survive.[20,22,23] Among the different Cop proteins, CopK is a periplasmic low molecular mass protein that is highly expressed in the presence of Cu(II) and has not been reported in any other copper-resistance mechanism.[23,25] CopK contains seven methionine residues, which are common ligands to Cu(I),[26] suggesting CopK is a copper-binding protein. CopK is the major periplasmic protein during copper challenge, but its exact function is unknown. It may serve as a periplasmic metallochaperone or as a copper-sequestering protein. In an attempt to characterize the molecular and functional properties of this protein, we have investigated its three-dimensional structure and its interaction with copper by NMR and mass spectrometry.

Results

Copper-induced expression of CopK

In the presence of copper, it has been demonstrated that *C. metallidurans* CH34 expresses CopK, a small periplasmic protein.[20] The dose-dependence of the copper effect on CopK expression was analyzed by Western blot using a polyclonal anti-CopK antibody. As shown in Fig. 1, expression of CopK increases with the concentration of copper in the medium, up to about 0.8 mM. Moreover, an induction of CopK was observed after 1 h of culture in the presence of 0.6 mM copper (data not shown).

Over-expression, purification and oligomerization state of apo-CopK

The gene coding for CopK has been cloned in a pET30b expression vector with its native leader sequence and the corresponding protein was exported correctly to the *E. coli* periplasm, as judged from SDS/PAGE analysis. After recovery of the periplasmic fraction, the protein was purified to homogeneity by gel-filtration on a Superdex-75

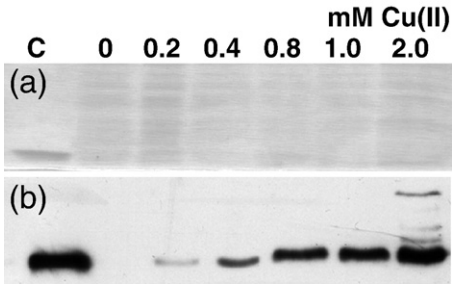

Fig. 1. Expression of CopK as a function of Cu(II) concentration. *Cupriavidus metallidurans* CH34 was grown under aerobic conditions at 30 °C during 24 h in minimal medium containing 0.2 % (w/v) gluconate and supplemented with increasing amounts of $CuCl_2$, and 10 μg of each extract were submitted to SDS-PAGE (15% polyacrylamide gel). (a) Gels stained with Coomassie brilliant blue R-250; (b) detection of CopK by Western blot, realized using a rabbit polyclonal anti-CopK antibody. Bands observed at high molecular mass do not correspond to oligomeric forms of CopK as they persist after incubation of the antibodies with purified CopK (for more details, see Materials and Methods). The control (C) corresponds to purified recombinant CopK protein (0.1 μg).

column. A yield of about 25–30 mg of pure protein per liter of culture in minimal medium was routinely obtained. Electrospray ionization mass spectrometry (ESI-MS) was used to determine the molecular mass of apo-CopK to 8279.58±0.06 kDa, corresponding to the sequence between Val21 and Gly94 of UniProtKB/TrEMBL entry Q58AD3. This confirmed correct cleavage of the native leader sequence by the *E. coli* host. In what follows, the CopK sequence numbering is that of the mature protein, running from Val1 to Gly74. The extent of isotopic labeling was determined by comparison of the molecular mass of pure unlabeled CopK with that of the labeled proteins. The extent of labeling was >97% for ^{15}N and ^{13}C. Purified apo-CopK showed an apparent molecular mass of 15 kDa on a Sephacryl S-100HR support. Therefore, analytical ultracentrifugation experiments were conducted on apo-CopK by varying the sample concentration between 3.4 μM and 1250 μM. The experimentally determined sedimentation coefficients, $\bar{s}$, are shown as a function of sample concentration in the Supplementary Data (Fig. S1). From these data, the dissociation constant of the dimer to monomer transition of apo-CopK can be estimated to be in the 10^{-5} M range.

Copper-binding by CopK

CopK being a protein expressed during the process of copper-detoxification, we first addressed its ability to bind copper by following the interaction of CopK with Cu(I) and Cu(II) by mass spectrometry and NMR (Fig. 2). In order to analyze the metal-binding properties of CopK by ESI-MS, nondenaturing conditions compatible with ESI mode and with the protein stability (50 mM ammonium acetate, pH 6.8) were used. Fig. 2a and b represent the ESI-MS partial profiles for the copper (I) and (II) titrations. For purposes of clarity, only the peak with charge +6 (m/z 1380.87 for apo-CopK) is shown. Titrating CopK with Cu(I) showed subsequent appearance of two new peaks at m/z 1391.12 Da and 1401.43 Da corresponding to the mass of apo-CopK +62.5±0.04 Da and apo-CopK +124.8±0.2 Da, respectively, at one and two molar equivalents of Cu(I) added to the protein (Fig. 2a). It should be noted that in both cases the transformation was quantitative, indicating two different binding sites with the second site having a lower Cu(I)-affinity than the first. Increasing the copper/protein ratio to 4 did not alter the spectrum anymore. A quantitative analysis of the binding affinity of CopK for Cu(I) was obtained by comparing the signal intensities for the apopeptide and the adduct peaks.[27] In order to calculate the relative amounts of apo-CopK and Cu(I)-CopK, the signal intensities for these species were summed for all charges as described in Materials and Methods. The experimentally determined amounts of apo-CopK and Cu(I)-CopK are shown as a function of total copper concentration in the Supplementary Data (Fig. S2). These data indicate that the Cu(I) affinity for the first Cu(I)-site can be described by $K_d < 0.5\ \mu M^{-1}$. Moreover, a drastic modification of the charge distribution in the mass spectra was observed in the presence of Cu(I) suggesting a significant conformational modification of CopK (data not shown).

A different behavior was found for Cu(II)-binding. The peak corresponding to apo-CopK (m/z 1380.86) disappears only after addition of two molar equivalents of Cu(II), and at four molar equivalents, two different forms of the protein were detected ($z=6$, $m/z=1391.72$, $m/z=1401.60$), corresponding to CopK bound to one or two copper-ions. These results clearly show a lower affinity of CopK for Cu(II) characterized by a K_d of 1 μM and may suggest that at least binding of the second Cu(II) is non-specific. Other experiments showed that a single Ag(I) could be bound by CopK but with significantly lower affinity than Cu(I). No CopK-metal complex was observed in the presence of ten equivalents of Ni(II) or Zn(II), suggesting copper specificity (data not shown).

NMR spectroscopy was used to monitor Cu(I) and Cu(II)-binding with a per-residue resolution. Fig. 2c and d show the superposition of the $^{1}H,^{15}N$- heteronuclear single quantum coherence (HSQC) spectra of CopK before and after addition of one molar equivalent of Cu(I) or Cu(II). Interaction with one molar equivalent of diamagnetic Cu(I) induces shifts of nearly all peaks in the $^{1}H,^{15}N$-HSQC spectrum, confirming the major conformational modification observed by ESI-MS due to Cu(I)-binding (Fig. 2c). Upon further titration of Cu(I) to CopK, peaks do not shift any more but a significant number broaden to below the level of detection (HSQC spectra are provided as Supplementary Data). As these experiments have been performed in the presence of a tenfold molar excess of sodium ascorbate and under a nitrogen atmosphere, we can reasonably exclude oxidation of Cu(I) to paramagnetic Cu(II).

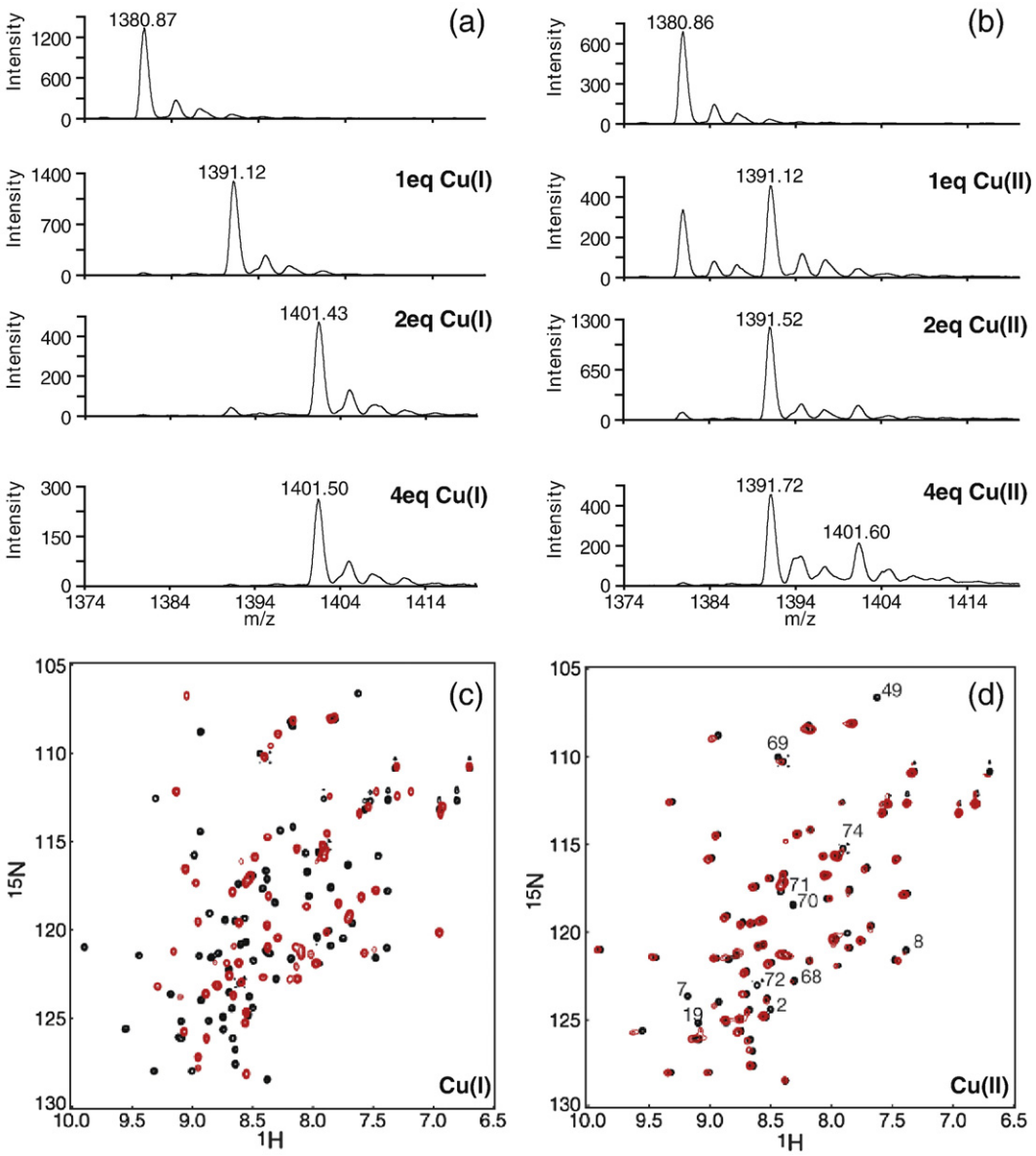

Fig. 2. Copper binding by CopK. Cu(I) and Cu(II) binding by CopK was followed by mass spectrometry and NMR. (a and b) Partial ESI-MS signals ($z=6$) of 1 μM CopK in the presence of increasing concentrations of (a) Cu(I) ($CuCl_2$+ ascorbic acid) and (b) Cu(II). The metal proportions are indicated in equivalents of metal ions/CopK monomer. (c and d) $^{1}H,^{15}N$-HSQC spectra, acquired in the absence (apo-CopK, black contour lines) and in the presence of one molar equivalent of Cu(I) (c) or Cu(II) (d) (red contour lines) at 25 °C. The protein concentration was 0.36 mM. Peaks with significantly reduced intensity after addition of paramagnetic Cu(II) are labeled by residue number. All spectra have been acquired in 50 mM ammonium acetate, pH 6.8.

On the other hand, addition of paramagnetic Cu(II) to apo-CopK does not affect the peak positions significantly but leads to a signal decrease for several residues due to enhanced relaxation by the spin of the unpaired electron. This indicates that the structure of Cu(II)-bound CopK is globally the same as that of apo-CopK. The peaks that are most affected are highlighted in Fig. 2d. They correspond to residues close to His19 and His70 in the apo-CopK structure (see below). Histidines are well-known to bind Cu(II). However, in the apo-CopK structure (see below), the two histidines are spatially separated and cannot form a single Cu(II)-binding site within the same subunit. On the other hand, a specific intermolecular binding site is not compatible with the observed ESI-MS spectra corresponding to a monomeric subunit with one Cu(II) ion bound. Together with the lower affinity of CopK for Cu(II) ($K_d=1$ μM), this is in favor of a rather non-specific binding and raises the question of whether the interaction with Cu(II) is of physiological relevance.

Solution structure of *apo*-CopK

Nearly complete ^{1}H, ^{13}C and ^{15}N resonance assignments could be obtained using a series of two- and three-dimensional NMR experiments as described in Materials and Methods. An assigned $^{1}H,^{15}N$-HSQC

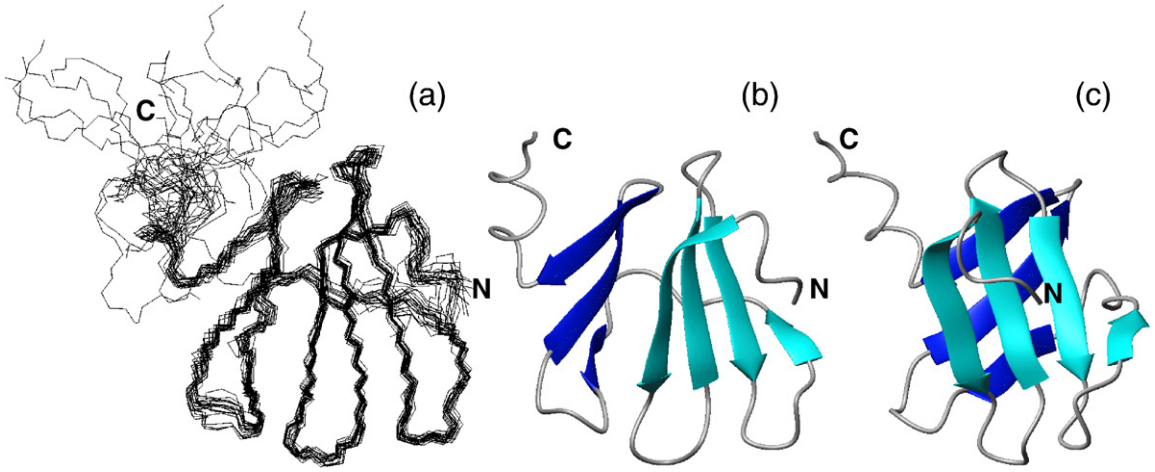

Fig. 3. Solution structure of apo-CopK. (a) Structural ensemble of 20 structures superimposed with respect to the mean structure. (b and c) Ribbon diagrams of the mean structure in two orientations differing by a rotation of 50° around the *y*-axis. The N- and C-terminal β-sheets are shown in cyan and blue, respectively.

spectrum can be found in the Supplementary Data (Fig. S3A).

A first structural ensemble was calculated from 1233 intra-subunit nuclear Overhauser effect (NOE) distance restraints, assigned using the ATNOS/CANDID programs,[28,29] and completed manually, as well as 58 dihedral restraints deduced from backbone chemical shifts. Isotope-filtered NOE spectrometry (NOESY) experiments were performed on a sample containing a mixture of $^{14}N,^{12}C$- and $^{15}N,^{13}C$-labeled protein to obtain inter-subunit distance constraints. However, unambiguous assignments were difficult to obtain from the 2D NOESY experiment and the signal to noise ratio was very low. Therefore, we decided to calculate the subunit structure by discarding possible inter-subunit NOEs. After water refinement, this ensemble was used to calculate the axial and rhombic components of the alignment tensor for apo-CopK suspended in a liquid-crystalline medium consisting of a mixture of 5% (v/v) pentaethyleneglycol monododecyl ether (C12E5) and hexanol.[30] The program Module[31] was used to estimate the alignment tensor parameters from 97 experimentally determined residual dipolar couplings (RDCs) and the ten best NMR structures. This also allowed validation of the monomeric structures by independently obtained experimental data. For calculation of the final structural ensemble, the 97 RDCs were introduced together with the distance and the dihedral restraints. After refinement in explicit water, the final structural ensemble comprised 20 structures, which are shown superimposed in Fig. 3a. The structural statistics are given in Table 1. The structure is well defined with a mean backbone rmsd of 0.53 Å. The protein is composed of two antiparallel β-sheets and could be classified as an open barrel (Fig. 3b and c). The two sheets are formed by residues 6–11, 17–21, 26–29, 35–36 (β-I to β-IV) and by residues 43–45, 51–55, 58–61 (β-V to β-VII), respectively. In β-barrel structures, the two sheets are usually connected by hydrogen bonds. In apo-CopK however, there is only one close contact between backbone atoms of the two sheets that involves the loops between strands β-I and β-II, and between strands β-V and β-VI. A hydrogen bond

Table 1. Statistics for the final structural ensemble (20 structures)

Coordinate precision (residues 6–61)		
rmsd for C′, C^{α}, N (Å)	0.53±0.14	
rmsd for heavy atoms (Å)	0.96±0.15	
Structural statistics		
Energy		
Bond (kcal/mol)	33.98±2.35	
Angle (kcal/mol)	140.48±12.11	
Improper (kcal/mol)	81.68±9.87	
Dihedral (kcal/mol)	358.77±4.38	
VDW (kcal/mol)	–182.26±18.21	
Electrostatics (kcal/mol)	–3081.13±55.9	
Violation energy (kcal/mol)	200.99±33.67	
Total (kcal/mol)	–2447.40±30.05	
rmsd from idealized geometry		
Bond lengths (Å)	0.0054±0.0002	
Bond angles (°)	0.662±0.028	
Improper angles (°)	1.835±0.133	
Experimental statistics	Number of restraints	rmsd
Distance restraints (Å)	1233 (892+341)[a]	0.0049±0.002
Dihedral restraints (°)	58	0.565±0.3
$rdc_{HN,N}$ (Hz)	49	1.115±0.948
$rdc_{C'C\alpha}$ (Hz)	48	0.543±0.763
Ramachandran statistics (PROCHECK) (residues 6 – 61)		
Residues in most favored regions (%)	88.9	
Residues in additional allowed regions (%)	7.7	
Residues in generously allowed regions (%)	1.6	
Residues in disallowed regions (%)	1.8	

[a] Unambiguous and ambiguous restraints, respectively.

from the amide proton of Arg47 to the carbonyl group of Asp11 is found in all 20 structures. In addition, a second hydrogen bond from Gln13-HN to Glu45-O is present in nine out of 20 structures. Residues Asn37 to Lys42 have an extended backbone conformation and form a linker between the two β-sheets. The C-terminal region (Glu64 to Gly74) appears disordered but with some helix-forming tendency for residues Glu64 – Arg67.

R_1, $R_{1\rho}$, and R_2 ^{15}N-relaxation rates and heteronuclear-NOE (hetNOE) were measured using ^{15}N-labeled protein samples at 0.3 mM, 1.3 mM and 1.5 mM concentration. Fig. 4 shows the different relaxation rate constants determined for the 1.3 mM sample as a function of the protein sequence. Relaxation rates could be calculated for 62 out of 74 residues and were found to be independent of protein concentration. The relaxation profiles show that the central part of the protein is quite homogenous whereas the N- and especially the C-terminal residues are much more mobile. This demonstrates that the conformational disorder observed within the structural ensemble for residues Glu64 – Gly74 is due to increased backbone mobility. In addition, the somewhat lower hetNOE and R_2 values observed for the residues belonging to the loop connecting β-strands IV and V (Asn37 – Glu40) indicate increased backbone mobility and correlate well with the observed rmsd values between 0.65 Å and 0.95 Å. In the secondary structure elements, the hetNOEs are found between 0.6 and 0.95, the highest values being obtained for the central β-strand of the second sheet (residues Lys51 – Lys55). Note, however, the higher error bars determined for the C-terminal β-sheet, which reflect the significantly lower signal intensity of the corresponding peaks in the ^{1}H,^{15}N-HSQC spectrum. This suggests the presence of dynamics on a milli- to microsecond timescale, which contributes to the transverse relaxation rates. Fig. 4d shows the difference between transverse relaxation rate constants obtained applying either the CPMG sequence ($R_{2,CPMG}$) or the ^{15}N spinlock field ($R_{2,R1\rho}$) during the

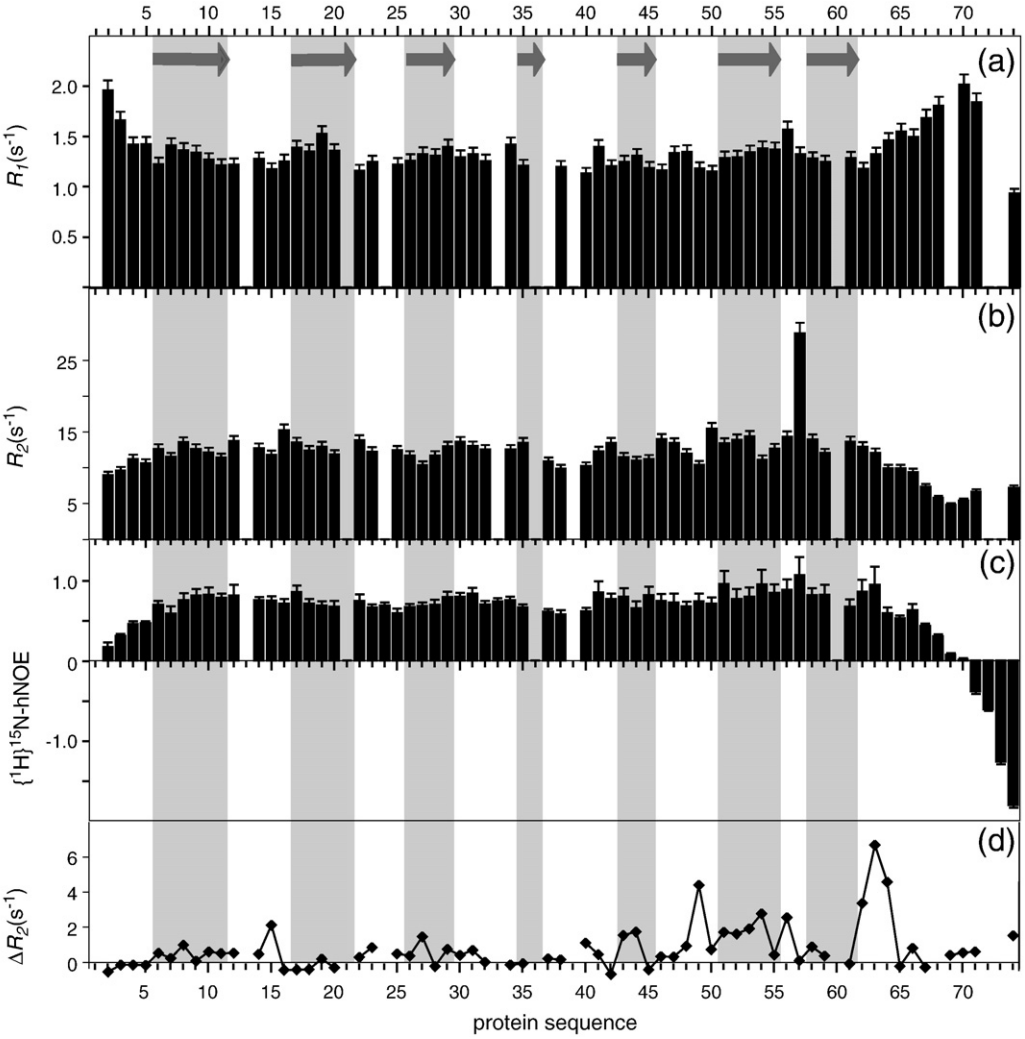

Fig. 4. ^{15}N-relaxation of apo-CopK. Longitudinal (a) and transverse (b) relaxation rates as well as the {^{1}H}^{15}N-heteronuclear NOE (c) are shown as a function of protein sequence. The position of the β-sheets within the protein is highlighted. Transverse relaxation rates were calculated from $R_{1\rho}$ relaxation rates as described in Materials and Methods. (d) Difference between $R_{2,CPMG}$ and $R_{2,R1\rho}$ relaxation rates that reflect contribution of chemical exchange to the R_2 relaxation rates.

relaxation period. Positive values indicate a contribution of chemical exchange to transverse relaxation. Significant differences are observed for residues at the transition between the structured and the completely unstructured part. Asn57 shows the highest R_2 rate constant and the corresponding crosspeak is hardly detectable in the $^{1}H,^{15}N$-HSQC spectrum. Backbone motions of these residues are certainly on an intermediate timescale. However, non-negligible values are also found for β-strands V and VI, and the loops connecting β-strands V, VI and VII. The latter observation is surprising, as this part of the protein appears to be well defined throughout the structural ensemble with numerous NOEs involving hydrophobic sidechains (Ile52, Ile53, Ile59, and Phe60).

To get more detailed information on protein mobility, we characterized the rotational diffusion properties of apo-CopK. Analysis of the ratio of R_2 and R_1 relaxation rates provides information on the size and the shape of a protein. For an isotropic molecule, this ratio is related directly to the molecular size. In the case of anisotropic overall reorientation, the R_2/R_1 ratio also depends on the orientation of the individual amide bonds within the frame of the rotational diffusion tensor, which by itself is determined by the molecular shape. The diffusion tensor of apo-CopK was determined from the R_1 and $R_{2,R1\rho}$ rate constants of residues 6 – 36 and 41 – 61 with the exception of residue 57 using the Tensor2 program.[32] The first structure from the NMR ensemble was used as a representative structure because this structure had the lowest rmsd with respect to the mean structure. Fitting the relaxation data assuming an isotropic global reorientation gives a rotational correlation time of 9.48±0.05 ns. This value is much too high for a monomeric protein with the mass of CopK (8279 Da) for which a correlation time of 5.3 ns could be estimated using HydroNMR.[33] Thus, the ^{15}N relaxation data are in good agreement with our previous observations that, at millimolar concentrations, apo-CopK is a dimer in solution.

However, in the case of apo-CopK, the measured R_2/R_1 ratios cannot be satisfactorily reproduced assuming isotropic molecular reorientation and we therefore analyzed the anisotropy of the diffusion tensor. The experimental data were best reproduced using an axially symmetric diffusion tensor with $D_{\parallel}=2.17\pm0.06\times10^{7}\ s^{-1}$ and $D_{\perp}=1.55\pm0.03\times10^{7}\ s^{-1}$ (prolate model) or assuming completely anisotropic diffusion:

$$D_{XX}=1.48\pm0.05\times10^{7}\ s^{-1}$$
$$D_{YY}=1.63\pm0.05\times10^{7}\ s^{-1}$$
$$D_{ZZ}=2.13\pm0.06\times10^{7}\ s^{-1}$$

The improvement of the fit due to the more complicated model was not statistically significant (*F*-test) and we therefore conclude that the axially symmetric prolate model best describes the overall tumbling of apo-CopK. Fig. 5 shows the molecular coordinates of the representative apo-CopK structure within the frame of the axially symmetric diffusion tensor. It can be noticed that the shape of the monomeric apo-CopK NMR structure is nearly globular and the determination of the rotational diffusion tensor for the structured part of mono-

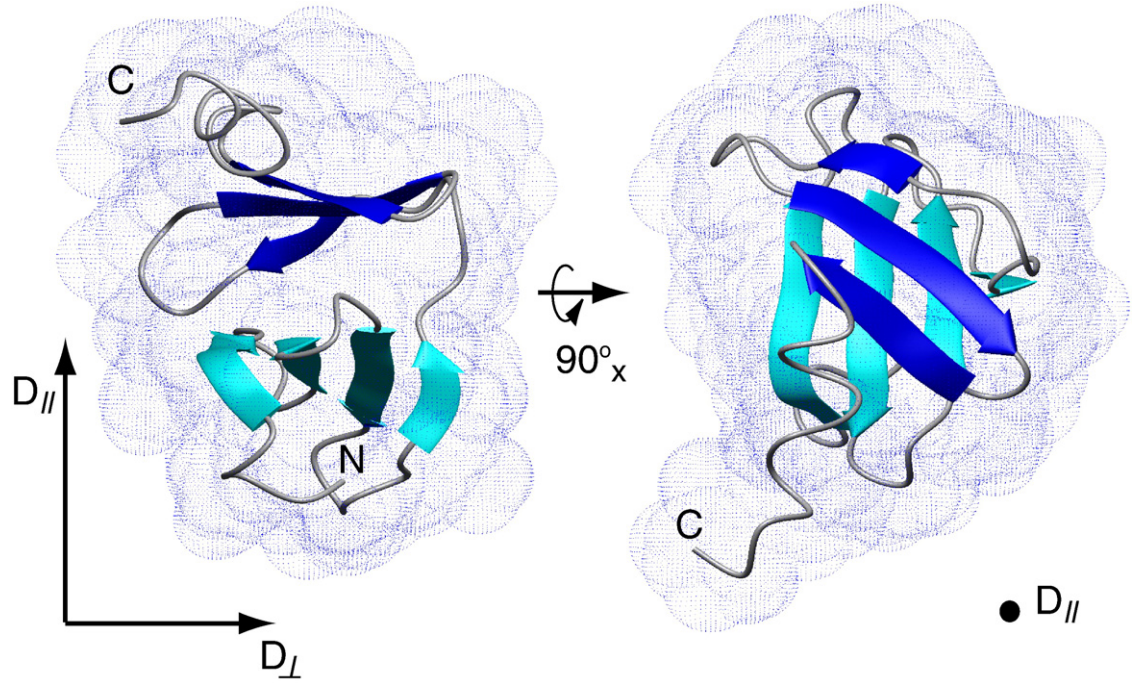

Fig. 5. The apo-CopK structure in the frame of the axially symmetric rotational diffusion tensor. The structure is shown in two different orientations with $D_{\parallel}$, the unique axis of the diffusion tensor lying vertically in the plane (left) or pointing out of the plane (right). The length of the arrows is proportional to the principal components $D_{\parallel}$ and $D_{\perp}$ ($D_{\parallel}/D_{\perp}=1.41$).

meric apo-CopK (residues 1–63) using HydroNMR results in a $D_{\parallel}/D_{\perp}$ ratio of 1.1. This does not agree with the $D_{\parallel}/D_{\perp}$ ratio of 1.41 determined from the experimental ^{15}N-relaxation data. The increased overall correlation time and the discrepancy of the diffusion tensor determined from the experimental data or from the monomeric *apo*-CopK structure support our previous findings that apo-CopK is a dimeric protein at millimolar concentrations. Moreover, the orientation of $D_{\parallel}$ with respect to the molecule indicates that the dimer interface would correspond roughly to the surface formed either by the N- or the C-terminal β-sheet (Fig. 5).

Hydrogen exchange and conformational stability

Hydrogen/deuterium exchange (H/D exchange) of amide protons occurs when the amide moiety is in a solvent-accessible and exchange-competent state. In well-structured proteins, and especially in secondary structure elements in which amide protons are mostly involved in hydrogen bonds, solvent exchange can occur only when the exchange-protecting structures transiently break, due to local or global unfolding fluctuations. Therefore, H/D exchange is related to the conformational stability of proteins. Under so-called EX2 conditions that are generally found at neutral pH, a thermodynamic equilibrium constant $K_{op}=k_{op}/k_{close}$ can be determined from the measured H/D exchange rates.[34] H/D exchange rate constants were measured for apo-CopK by rapidly dissolving the protein in $^{2}H_2O$ and following site-resolved intensity decay in a series of 2D SOFAST heteronuclear multiquantum coherence (HMQC) spectra of ~7 s per spectrum.[35] This allowed quantification of exchange rate constants of up to ca 0.1 s^{-1}. Fig. 6 shows the equilibrium constant K_{op} as a function of protein sequence. It can be seen that in the secondary structure elements, H/D exchange is significantly slowed by interstrand hydrogen bonds. The periodicity observed in strands I and V reflects the orientation of the HN bonds towards the neighboring strand (low K_{op}) or the outside of the β-sheet (high K_{op}). Comparing the K_{op} constants determined for the individual β-strands, we find that the most stable hydrogen bonds are formed between strands β-I and β-II (HN groups of residues 10, 12, 18 and 20) with K_{op} values around 2×10^{-4}, whereas contacts between the last two β-strands are characterized by K_{op} values around 8×10^{-4} (HN groups of residues 53, 55, 58 and 60). Overall, amide protons from residues involved in interstrand hydrogen bonds in the N-terminal β-sheet seem to be more protected from solvent exchange than those within the C-terminal sheet, suggesting that the C-terminal β-sheet is more subjected to protein unfolding fluctuations.

Cu(I)-CopK characterization by NMR

To get closer insight into the conformational changes upon Cu(I) binding, we assigned the backbone resonances of CopK in the presence of 1 mol. eq. of Cu(I). NH assignments could be made for 56 out of 74 residues. Cross-peaks corresponding to residues 1, 2, 7, 18, 29, 55–62 and 68–71 could not be identified in the HSQC spectrum due to either chemical exchange or increased solvent exchange. In order to assess the structural compactness in Cu(I)-CopK, we performed two-dimensional HET-SOFAST experiments[36] on Cu(I)- and apo-CopK. These experiments allow quantification of the proton cross-relaxation efficiency observed between a given amide proton and aliphatic protons. This efficiency is determined by the number and proximity of neighboring protons as well as by local dynamics. Thus, HET-SOFAST

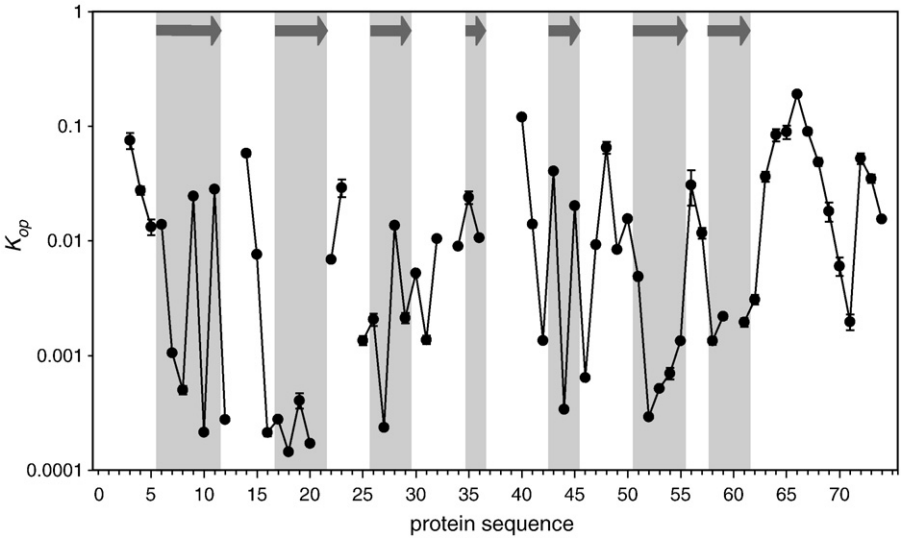

Fig. 6. H/D exchange of amide protons in apo-CopK. The thermodynamic equilibrium constant K_{op} is shown on a logarithmic scale as a function of protein sequence. The position of the β-sheets is highlighted. K_{op} has been calculated from the measured H/D exchange rates assuming an EX2 limit (see the text). The H/D exchange rates have been measured at pH 6.5 and at 24 °C as described in Materials and Methods.

data give insight into the structural compactness as seen by amide proton sites. The observed parameter, λ_{NOE}, which is given by the intensity ratio of an aliphatic-saturated and a reference spectrum, falls in the range 0.1–0.3 for compact, well-folded proteins, whereas values of 0.6–0.8 are observed for totally unfolded polypeptides. Average λ_{NOE} values were 0.28 and 0.43 for apo-CopK and Cu(I)-CopK, respectively, demonstrating that Cu(I)-CopK is less compact than apo-CopK. Backbone carbon chemical shifts are related to the presence of secondary structure elements.[37] Comparison of the values measured

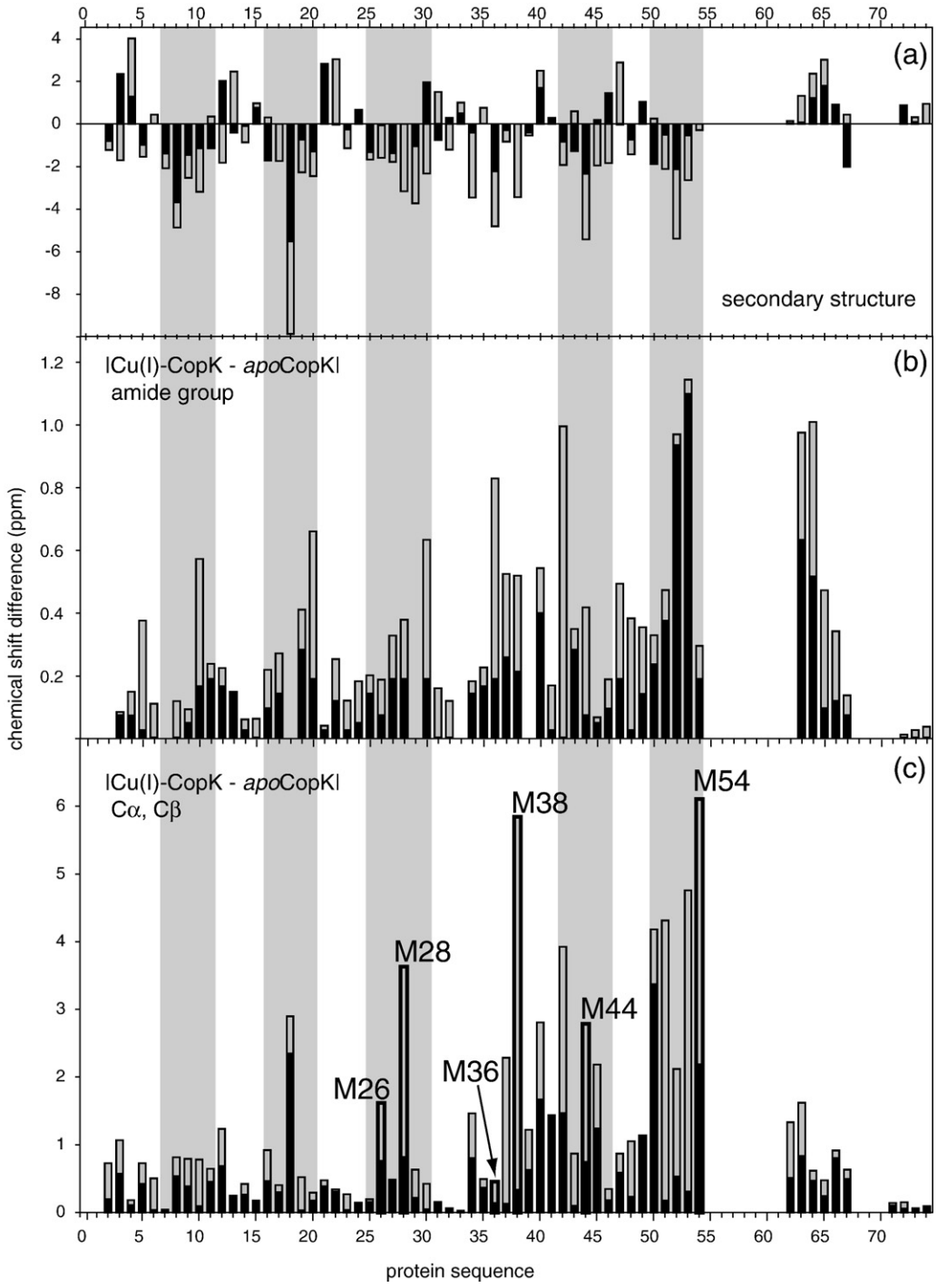

Fig. 7. Secondary structure of Cu(I)-CopK and comparison with apo-CopK. (a) Differences between the chemical shifts measured for Cu(I)-CopK and those expected for a completely unstructured protein for C^{α} (gray bars) and C′ (black bars). Stretches with negative values indicate β-strand structures that are highlighted. (b and c) Chemical shift differences between apo-CopK and Cu(I)-CopK in absolute values for (b) backbone amide groups (HN, gray bars and $(\gamma_N/\gamma_H)x\Delta^{15}N$, black bars), and (c) backbone carbons (expressed as $(\gamma_C/\gamma_H)x\Delta^{13}C$; C^{α}, black bars and C^{β}, gray bars). All values are given in ppm. No amide resonances could be observed for residues 1–3, 55–62 and 68–71 in Cu(I)-CopK (see the text). Methionine residues are highlighted because of their possible role as Cu(I)-ligands.

for Cu(I)-CopK and those expected for a completely unstructured protein reveals the presence of five β-strands, corresponding to strands I–III and V-VI in apo-CopK (see Fig. 7a). No $^{1}H,^{15}N$-cross-peak could be detected in the $^{1}H,^{15}N$-HSQC spectrum for residues located in the C-terminal β-strand (β-VII) in apo-CopK and we suppose that binding of Cu(I) destabilizes the C-terminal β-sheet with a loss of defined secondary structure for the last strand. Fig. 7b and c show the backbone chemical shift differences between apo- and Cu(I)-CopK that can be related to structural differences between the two forms. It can be seen that the C-terminal half of the protein undergoes the most significant conformational changes upon copper-binding. Note the large chemical shift differences for the C^{β} atoms of Met28,

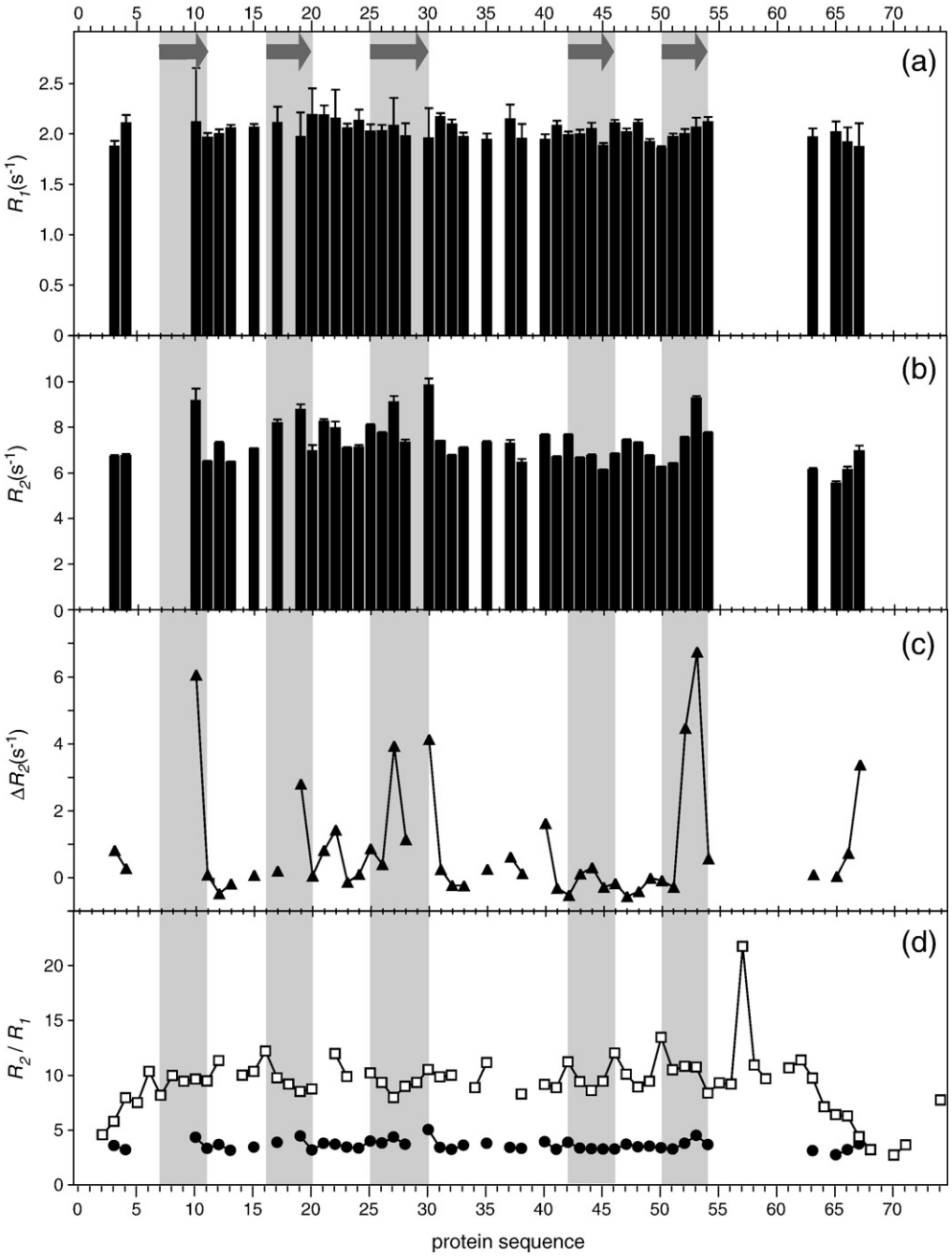

Fig. 8. ^{15}N-relaxation of Cu(I)-CopK. Longitudinal (a) and transverse (b) relaxation rates are shown as a function of protein sequence. Transverse relaxation rates were calculated from $R_{1\rho}$-relaxation rates as described in Materials and Methods. (c) Contribution of chemical exchange to the transverse ^{15}N-relaxation shown by the difference between $R_{2,CPMG}$ and $R_{2,R1\rho}$ relaxation rates. (d) $R_{2,R1\rho}/R_1$ ratio for apo-CopK (open squares) and Cu(I)-CopK (filled circles). The $R_{2,R1\rho}/R_1$ ratio is related to the overall correlation time (τ_c) and therefore to the size of the molecule. Note the significant difference of more than a factor of 2 between the two forms of CopK. The position of the β-sheets within Cu(I)-CopK is indicated by gray boxes.

Met38 and Met54, which suggests that the side-chains of these residues are part of the Cu(I) binding-site. A $^{1}H,^{15}N$-HSQC experiment optimized for the detection of $^{2}J_{NH}$ couplings in the imidazole ring was performed on apo and Cu(I)-CopK to investigate whether one of the two histidines (His19 and His70) was involved in Cu(I) coordination. In the case of His70, the frequencies of both nitrogens were found to be below 200 ppm for apo and Cu(I)-CopK, indicating that His70 was in the charged form in both protein samples.[38] In the case of His19, $N^{\varepsilon 2}$ appeared protonated in both protein samples, whereas the $N^{\delta 1}$ resonance was broadened and detected at 217 ppm and 234 ppm for apo and Cu(I)-CopK, respectively, suggesting partial protonation that was more pronounced for the apo protein. The observed chemical shift difference could be attributed to a lower pH in the apo-CopK sample, resulting from lyophilization in ammonium acetate buffer (pH 5.5 – 6.0 compared to 6.8 for Cu(I)-CopK). Despite the slightly different sample conditions, these results suggest that neither of the two histidines present in the CopK sequence is involved in Cu(I) coordination. The chemical shift of an imidazole nitrogen coordinated to Cu(I) is expected at 220 ppm,[39] which is not observed for the Cu(I)-bound protein.

With the aim of obtaining better insight into protein mobility, longitudinal and transverse relaxation rates were measured for Cu(I)-CopK (see Fig. 8). As for apo-CopK, transverse relaxation rates were determined both using CPMG-type and $R_{1\rho}$-type relaxation experiments. The profile of the longitudinal relaxation shown in Fig. 7a is flat and does not indicate any region with increased mobility in the fast motional range, this holds also for the C-terminal residues that were highly flexible in apo-CopK. On the contrary, several residues show increased $R_{2,R1\rho}$ values and significant differences between $R_{2,CPMG}$ and $R_{2,R1\rho}$ relaxation rates (Tyr10, His19, Asn37, Phe30, Ile52, and Ile53), indicating chemical exchange contributions to transverse relaxation. Fig. 7d shows the comparison of the $R_{2,R1\rho}/R_1$ ratio for apo-CopK and Cu(I)-CopK. In the absence of chemical exchange or increased internal motion, the mean value is proportional to the molecular size, whereas the amplitude of the fluctuations is related to the anisotropy of the diffusion tensor. It can be seen immediately that apo-CopK and Cu(I)-CopK differ in size, suggesting that Cu(I)-CopK is a monomer. This was confirmed by analytical ultracentrifugation (Cu(I)-CopK = 1.3 S at a concentration of 150 μM, as shown in the Supplementary Data). In addition, the nearly constant values of $R_{2,R1\rho}/R_1$ found for Cu(I)-CopK indicate that its shape should be roughly globular, whereas it has been demonstrated above that apo-CopK has the shape of an axially symmetric prolate. Cu(I)-binding to CopK therefore seems to induce major structural variations in the C-terminal part of CopK, which is accompanied by the destabilization of the tertiary structure and dissociation of dimeric apo-CopK.

Discussion

The gene coding for CopK, the periplasmic protein described in this work, is situated within the *cop* determinant on *C. metallidurans* CH34 plasmid pMOL30. This *cop* determinant, composed of 21 genes that are upregulated in the presence of external copper, is unique with respect to its complexity compared to other copper-resistance mechanisms described so far.[23] During copper challenge, CopK appears to be one of the major proteins in the periplasmic space, suggesting an important role in copper handling. Similarity searches using the Blast program reveal five significant hits within the UniProt Knowledgebase, which appear to be periplasmic proteins and show between 40 % and 50 % sequence identity with the processed CopK sequence. However, no physiological function has so far been assigned to these proteins. The sequence alignment can be found in the Supplementary Data. It is interesting to note that all organisms containing a CopK-analog are soil bacteria, able to degrade or metabolize organic or aromatic compounds. Some of these organisms, including *C. metallidurans* CH34, have been isolated from industrial environments and may have adapted to cope with simultaneous contamination by organic solvents and heavy metals. This would suggest a possible transfer of copper-resistance genes between the different species colonizing these biotopes, a hypothesis that is strengthened by the simultaneous occurrence of other *cop* orthologs in *Acidovorax* sp., *Polaromonas naphthalenivorans*, *Rhodoferax ferrireducens*, and *Dechloromonas aromatica* genomes in the vicinity of the *copK* ortholog. Assuming that the CopK-like proteins have conserved function, analyzing sequence conservation can provide indications on functionally or structurally important residues. It can be seen from Fig. S4 that five of the seven methionines of *C. metallidurans* CopK are conserved (Met26, Met28, Met38, Met44 and Met54) in five of the six sequences, the only exception being the hypothetical protein from *Delftia acidovorans* SPH-1, which has the least sequence similarity compared to CopK. This points to a functional importance of these methionine residues. Indeed, in several small periplasmic copper chaperones such as CopC, PcoC and CusF, Cu(I) is bound in three-coordinate sites with at least two thioethers involving methionine sidechains.[40–42] An additional ligand usually is contributed by the more electron-donating imidazole ring of a histidine. Inspection of the sequence alignment reveals that His70, which is situated in the unstructured C-terminal region of CopK is present in five of the six sequences. However, the chemical shifts of the imidazole nitrogens measured for Cu(I)-CopK did not support the coordination of Cu(I) by any of the two histidines, and additional experimental data are required for the identification of the Cu(I)-binding site in CopK. Besides these residues possibly involved in metal-binding, a conserved stretch of seven residues (Phe21 – Gly27) can be identified that forms a

charged, surface-exposed loop connecting β-strands β-II and β-III. The surface formed by these residues is contiguous with the exposed parts of Met26 and Met54, suggesting that they have a role in the intermolecular transfer of Cu(I).

Structural studies of copper chaperones and metal-binding P-type ATPase domains from different organisms have provided a wealth of information on these small proteins implicated in intracellular copper transfer.[43] Whereas cytoplasmic copper chaperones are characterized by an αβ ferredoxin-like fold with Cu(I) bound to an MXCXXC motif,[43] the few, small periplasmic copper-binding proteins described so far differ in several aspects: they are all-β proteins and they bind Cu(I) in a three or four coordinate site involving methionine sidechains.[40–42,44–47] *E. coli* PcoC and its *P. syringae* ortholog CopC are β-barrel proteins with a Greek-key topology that resembles the so-called rubredoxin fold.[41,44,46] They bind Cu(I) and/or Cu(II) in distinct sites, highly specific for the oxidation state.[41,45,48] Crystal structures of the Cu(I)Cu(II)-loaded CopC protein were obtained under two different conditions and differ in the coordination chemistry at each copper-site, the conformation of metal-binding loops and the mode of interaction between CopC molecules. The low pH form shows head-to-head dimers in which the Cu(I) ion is localized at the interface, linked by four methionine sidechains provided by both subunits. In the high pH form, Cu(I) is coordinated by Met40 and His48 from the same subunit and a water molecule that lies on the crystallographic twofold axis.[41] X-ray absorption spectroscopy (XAS) of Cu(I)-CopC at pH 7.0 suggested Cu(I) coordination by two or three sulfur atoms and one histidine nitrogen. The presence of three sulfur atoms in the coordination sphere resulted in a slightly improved fit.[45] The Cu(I) affinity of CopC has been estimated from ligand competition experiments using the Cu(I)-specific ligand bathocuproïne disulfonate. These experiments provided a minimum value of K_d corresponding to 10^{-13} M.[41] Subsequently, PcoC was shown to have a twofold higher affinity for Cu(I).[48] The solution structure of another extracytoplasmic copper-binding protein, DR1885, functionally equivalent to eukaryotic Cox17 has been resolved and shown to have a fold similar to CopC/PcoC. This protein also binds Cu(I), probably by means of three methionines and one histidine as inferred from XAS data.[47] On the other hand, *E. coli* CusF, a periplasmic protein involved in copper and silver resistance, forms a five stranded β-barrel, classified as an OB-fold.[42] In this protein, Cu(I) or Ag(I) are coordinated by sidechain atoms from Met47, Met49 and His36 with an indole ring positioned above the metal ion. [49,50] Isothermal titration calorimetry was used to demonstrate that CusF bound Ag(I)- and Cu(I)-ions with high affinities that were characterized by dissociation constants of 38.5 nM and 495 nM, respectively.[51] More recently, CzcE, a periplasmic protein belonging to the *czc*-operon in *C. metallidurans* CH34, has been shown to bind Cu(I) and Cu(II) simultaneously.[52] The three-dimensional structure of this dimeric protein is unknown, but secondary structure prediction and preliminary NMR data suggest that CzcE also is an all-β protein but with a probably unstructured N-terminal extension. A large number of unstructured residues have been observed for CopH, a CzcE paralog.[53] In the present work, we describe the solution structure of apo-CopK, which probably is another periplasmic copper chaperone. Like the proteins described above, apo-CopK has an all-β fold, and the number as well as the conservation of several methionines in its sequence point towards their possible implication in metal binding. However, there is no significant structural or sequence homology with the other periplasmic copper chaperones. Concerning the overall fold, apo-CopK most closely resembles CusF, but CusF is a real β-barrel formed by two antiparallel β-sheets with the first strand being a component of both sheets and interactions between β-III and β-V that close the barrel. No such interaction can be observed in apo-CopK, in which the two sheets are rather planar and in a perpendicular arrangement (Fig. 3). The convergence of overall fold and metal-binding site among proteins from different organisms with related function but without significant sequence conservation is remarkable.

Since the topology of apo-CopK differs significantly from that of other known periplasmic copper chaperones, we used the Dali server† to search the Protein Data Bank for proteins with similar folds.[54] Surprisingly, only a single protein domain was identified that matches both β-sheets of CopK (PDB ID code 1VKY, *S*-adenosinylmethionine:tRNA ribosyltransferase isomerase, small domain, *Z*-score of 4.0 with rmd of 2.8 over 58 aligned residues). However, this domain again differs from apo-CopK by the fact that it is composed of a single, barrel-like β-sheet with extensive contacts between strands III and VI.

We observed that the oligomerization state of CopK was dependent on the occupancy of the first metal-binding site at NMR sample concentrations (10^{-3}–10^{-4} M). This was inferred from NMR relaxation and analytical ultracentrifugation studies with CopK in its apo and 1Cu(I)-bound states (Fig. 8d; Supplementary Data Fig. S1). The dissociation constant of dimeric apo-CopK was estimated to be in the range of 10^{-5} M. This relatively weak association can explain why a single, monomeric form of apo-CopK was detected by ESI-MS, even under mild experimental conditions. The physiological relevance of the dimeric apo-CopK remains uncertain. CopK has been shown experimentally to be one of the major periplasmic proteins in *C. metallidurans* CH34 under copper stress (R. W., unpublished results), but only a small fraction may be in the apo form due to the presence of periplasmic copper.

However, dimerization of periplasmic copper chaperones has been reported. PcoC weakly associated in the apo and in the Cu(I)-bound form with association constants of 3×10^2 and 8×10^3 M^{-1}, respectively.[46] Analytical ultracentrifugation experiments indicated

† www.ebi.ac.uk/dali/index.html

that the orthologous protein CopC is monomeric in both states,[41] whereas NMR relaxation data suggested partial aggregation of the Cu(I)-bound form.[45] Crystal structures obtained of Cu(I)-bound PcoC differed for native and selenomethionine proteins, but in both crystal forms, the Cu(I)-binding site was involved in the dimer interface.[46] Similar intermolecular contacts were observed in different Cu(I)Cu(II)-CopC structures; however, the mode of interaction between subunits was dependent on the experimental conditions.[41] Taken together, these observations suggest that these periplasmic Cu(I)-binding proteins have a common tendency to form weakly associated dimers. As in the case of CopK, it is not known whether this is of any physiological relevance.

The fit of the ^{15}N-relaxation data to the three-dimensional structure of apo-CopK allowed to determine the rotational diffusion tensor for apo-CopK, which is related to the shape of the protein. The axially symmetric nature of this tensor gives experimental evidence for the location of the dimer interface (see Fig. 6). Most remarkably, comparison of the diffusion and the alignment tensors, calculated from independent ^{15}N-relaxation and RDC data respectively, shows that the principal axes of both tensors have nearly the same orientation with respect to the molecular frame (data not shown). As we expect the residual alignment of the protein in the steric alignment medium used (C12E5-hexanol) being determined mainly by the molecular shape, this observation provides additional evidence for the location of the dimer interface. Attempts to determine the three-dimensional structure of the dimeric apo protein failed, as only a few intersubunit NOEs could be detected in an isotope-filtered NOESY experiment. However, several experimental observations are consistent with a dimer interface being formed by the C-terminal β-sheet:. (1) The tentative assignment of the intersubunit NOEs; (2) the surface charge distribution in monomeric apo-CopK with a positively charged N-terminal side (exposed Lys17, Lys31, Lys34, His19 sidechains) and a more hydrophobic C-terminal surface (exposed Phe60, Ile53 and Val43 sidechains); (3) the increased R_2 rates observed for several residues in the C-terminal β-sheet, which can be explained by slow dimer–monomer transitions; and (4) the extent of the chemical shift changes observed for residues in the C-terminal half of the protein upon copper binding and resulting dimer dissociation. Unfortunately, the presence of the flexible C-terminal extension (residues 64–74) prevented the use of any rigid-body docking approach in order to determine a three-dimensional model for the dimeric apo-CopK structure.

Binding of the first Cu(I) to CopK was found to induce major conformational reorientation associated with dimer dissociation. From the comparison of the backbone chemical shifts between apo and Cu(I)-bound CopK it becomes evident that the most important structural changes occur in the C-terminal β-sheet which is disrupted upon Cu(I)-binding. We suggest that Cu(I)-binding, possibly involving Met54, induces reorientation of some residues situated in or close to the C-terminal β-strand. Met54 is a likely residue to be involved in this process because its β-carbon atom shows a large chemical shift variation upon metal binding. Reorientation of residues in or near the C-terminal β-strand then opens hydrogen bonds between strands β-VI and β-VII in the apo-form. Such a model is consistent with the hydrogen exchange measurements on apo-CopK that demonstrated the lower stability of hydrogen bonds between strands β-VI and β-VII. If the C-terminal strand is involved in the dimer interface, it is easy to imagine how partial loss of the three-stranded β-sheet (of which the C-terminal β-strand is a part) is likely to cause dimer dissociation directly.

Mass spectrometry and NMR showed that CopK can specifically bind up to two Cu(I) ions with high affinity. Complementary experimental data demonstrate an increase in chemical exchange by consecutive Cu(I)-binding: several ^{1}H,^{15}N-correlation peaks disappeared from the ^{1}H,^{15}N-HSQC spectrum and increased exchange contributions to transverse relaxation rates have been observed for numerous residues in the 1Cu(I)-bound form (Fig. 8c). We cannot exclude the possibility that an equilibrium between apo and Cu(I)-CopK contributes to the observed chemical exchange but the semi-quantitative measurement of protein compactness using HET-SOFAST experiments showed a global decrease of aliphatic proton density at the amide proton sites. Taken together, there is strong experimental evidence for an increase of the flexibility of CopK upon Cu(I) binding. Binding of the second copper further increases chemical exchange, as reflected by the disappearance of additional cross-peaks from the ^{1}H,^{15}N-HSQC spectrum (Supplementary Data Fig. S3B). The close coupling of proein oligomerization state to copper-loading and the apparent increase in protein plasticity in the metal-bound state may be related to a possible function of CopK as a copper transfer protein. This behavior would enable the protein to specifically interact with different partner proteins as a function of the number of copper ions bound. In addition, the enhanced protein flexibility in the metal-bound state could confer the ability to bind to several different target proteins, and especially to intrinsically flexible proteins as for example the large periplasmic methionine-rich repeat region of CopB. However, to date there is no experimental evidence that CopK is a copper chaperone and we cannot rule out a possible function as a copper buffering or sequestering protein.

Characterization of the structure and the metal-binding properties of CopK represents a first step in deciphering the complex response of *C. metallidurans* CH34 to copper on a molecular level. The molecular structure and the Cu(I)-binding site of 1Cu(I)-CopK are currently under investigation. Ongoing efforts also concentrate on the identification of the physiological partners of this protein in order to provide information on metal-trafficking pathways in the periplasm. In addition, specific

insertion mutants in different *cop* genes, including *copK* are being created. The phenotypic analysis of the corresponding mutant strains grown in media containing different amounts of copper and other heavy metals will contribute to assigning molecular functions to the individual *cop* proteins.

Materials and Methods

Expression and purification of the recombinant CopK protein

The plasmid pIRMWcopK1[25] was used to transform the phage T7 RNA polymerase-containing host *E. coli* BL21 (DE3). The freshly transformed bacteria were grown at 37 °C in M9 minimal mineral medium with glucose (4 g/L) as carbon source and supplemented with 0.1 mM $MnCl_2$, 0.05 mM $ZnSO_4$, 0.05 mM $FeCl_3$ and a vitamin solution as described.[55] Isotopically labeled protein was prepared by growing the cells with $^{15}NH_4Cl$ (1 g/L) and $^{13}C_6$-glucose (2 g/L) as sole nitrogen and carbon sources. Protein expression was induced by the addition of 0.5 mM isopropyl-1-thio-β-D-galactopyranoside when cells reached an A_{600} between 0.6 and 0.8. Cells were grown overnight at 20 °C and harvested by centrifugation. For the extraction of periplasmic protein, the pellet from 1 L of culture was suspended in 100 mL of extraction buffer (30 mM Tris–HCl (pH 8.0), 20% (w/v) sucrose, 1 mM EDTA) and incubated for 5 min at room temperature. Cells were pelleted by centrifugation at 10,000*g* for 10 min, re-suspended in 60 mL of ice-cold 5 mM $MgCl_2$ and incubated on ice for 10 min. After centrifugation at 10,000*g* for 20 min, the supernatant, corresponding to the periplasmic fraction was recovered, supplemented with Mes buffer (pH 6.0) to a final buffer concentration of 50 mM and concentrated to a minimal volume by ultrafiltration (Diaflo cell equipped with a YM-3 membrane or Ultra-15 centrifugal filter devices with a cutoff of 5 kDa, both by Amicon Co.). The protein solution was then subjected to filtration on a preparative Superdex-75 column (Amersham-Pharmacia Biotech.) previously equilibrated with the same buffer. Elution was run at 0.8 mL.min^{-1} and 1 mL fractions were collected. Fractions were assayed for protein by measuring absorbance at 280 nm, and for the presence of CopK by SDS/PAGE. The CopK-containing fractions were pooled, concentrated and stored at −80 °C. At this stage, CopK was electrophoretically pure. The yield for a typical purification procedure was 25–30 mg of pure CopK from 1 L of minimal medium.

Protein concentration was determined using bovine serum albumin as a standard and the Micro BCA protein assay (Pierce, Rockford, IL). All concentrations are expressed as subunit concentration. The native molecular mass was estimated by elution from a calibrated analytical Sephacryl S-100 HR filtration column. A Superdex-75 column could not be used because the protein was retained by this support.

For the preparation of Cu(I)-bound CopK for NMR studies, the protein was transferred to 50 mM ammonium acetate, pH 6.8. All solutions for the preparation of the Cu(I)-CopK complex were handled in a glove-box under a nitrogen atmosphere. Ten molar equivalents of sodium ascorbate (pH 8.0) prepared by titration of ascorbic acid with NaOH were mixed with the protein solution before addition of one or two molar equivalents of $CuCl_2$ dissolved in water. The sample was placed in an NMR tube hermetically closed with a rubber septum and was stable for at least two weeks.

Western blot analysis

C. metallidurans CH34 was grown under aerobic conditions at 30 °C for 24 h in minimal medium containing 0.2% gluconate and supplemented with 0, 0.2, 0.4, 0.8, 1 or 2 mM $CuCl_2$. Cell extracts were prepared using 40 mM Tris–HCl (pH 7.2), 8 M urea, 4% (v/v) Chaps, 2 mM tributyl phosphine, and Complete Mini EDTA-free Protease Inhibitor Cocktail (one tablet/mL; Roche). The proteins were resolved using SDS/PAGE (15% acrylamide) and transferred to a polyvinylidene difluoride membrane (Immobilon-P Transfer Membrane; Millipore, Chelmsford) by a semidry blotting system. The membrane was incubated for 1 h at room temperature with rabbit polyclonal anti-CopK antibody (1:250 (v/v) in TBS buffer containing 0.1% (v/v) Tween 20 and 1% (w/v) BSA). Rabbit anti-CopK antibody was generated with purified recombinant apo-CopK protein (Hormonology Laboratory, Marloie, Belgium). Horseradish peroxidase-conjugated antirabbit (Santa Cruz Biotechnology) was used as a secondary antibody at a dilution of 1:3000 (v/v). The antibody–protein complexes were visualized using ECL reagents (Amersham Biosciences). The specificity of anti-CopK antibodies was determined by control experiments in which the antibody solution was pre-incubated with 10 μg of purified CopK for 2 h at room temperature immediately before the Western blot. In these control experiments, the signal due to the presence of CopK disappeared, whereas unspecific bands at high molecular mass remained. Observation of these unspecific bands was not correlated with the presence of copper in the culture medium.

Mass spectrometry

Mass spectrometry experiments were conducted using a Q-TOF hybrid mass spectrometer (Q-tof II; Waters) equipped with an electrospray source (Z-spray) operated in positive-ion mode. The electrospray carrier solvent was either MS solution (50 mM ammonium acetate (pH 6.8) with or without 2 mM ascorbic acid) for measurements under non-denaturing conditions, or 0.2% (v/v) formic acid in 50% (v/v) acetonitrile for mass determinations of metal-free proteins. Green fluorescent protein (GFP) was used for mass calibration checks. Optimized conditions corresponded to a needle voltage of 3000 V and a cone voltage of 30 V, while the temperature source was held at 150 °C. Spectra were recorded by averaging 50 scans from 400–2000 m/z at a scan rate of 5 s/scan. Data analysis and convolution were performed using Masslynx 4.0 (Waters Micromass). Sample concentration was 1 μM or 8 μM in 50 mM ammonium acetate (pH 6.9) with or without 2 mM ascorbic acid and with the appropriate Cu(I) or Cu(II) concentrations (0.1, 0.2, 0.3, 0.5, 0.6, 0.7, 0.8, 1, 1.2, 1.3, 1.5, 1.6, 1.8, 2, 4 and 8 molar equivalents). To estimate the equilibrium constants for copper binding to apo-CopK, the signal intensities for the free and copper-complexed protein were summed for all charge states. It was assumed that the total signal response for each individual species was proportional to the concentration of that species in the gas phase, and by extension in solution. From these experiments, only the upper limit of the dissociation constant can be determined, as copper was quantitatively bound at all concentrations tested.

Analytical ultracentrifugation

Sedimentation velocity experiments were performed using a Beckman XL-I analytical ultracentrifuge and an

An-50-Ti rotor. Experiments were carried out at 20 °C in 50 mM sodium acetate, pH 6.8. Protein concentrations were 1250, 920, 845, 750, 500, 150, 76, 15, 7.3, and 3.6 μM for apo-CopK and 150 μM for Cu(I)-CopK. The latter sample also contained 15 mM sodium ascorbate and 150 μM $CuCl_2$. Samples were loaded into two-channel centerpieces equipped with sapphire windows and with 3 mm ($c \geq 150$ μM) or 12 mm ($c \leq 76$ μM) optical pathlength and centrifuged at 42,000 rpm overnight. Sedimentation profiles were recorded every 10 min for each cell at 228 nm ($c \leq 150$ μM) or 278 nm ($c \geq 500$ μM) and using interference optics. Data analysis was performed using the continuous distribution of sedimentation coefficients ($c(s)$) analysis with the software Sedfit V11.3, developed by P. Schuck§.[56] The $c(s)$ curves were obtained considering 200 particles with sedimentation coefficients (s) between 0.1 and 3 S (3.8 – 150 μM) or 0.5 S and 10 S (500–1250 μM). The partial specific volume of the protein (0.723 mL/g) was determined from the sequence with Sednterp softwareǁ.

The theoretical values of s were calculated for the monomer and dimer using the Svedberg's equation with $f/f_{min} = 1.35$, and corresponded to 1.12 S and 1.77 S, respectively.

NMR spectroscopy

All NMR experiments were performed on a Varian INOVA 600 spectrometer equipped with a triple-resonance (^1H, ^{13}C, ^{15}N) probe and shielded z-gradients, a Varian DirectDrive 600 or a Varian INOVA 800 spectrometer, the latter two equipped with (^1H,^{13}C,^{15}N) cryoprobes. NMR experiments were acquired at 25 °C with a typical sample concentration of 1.0–1.5 mM if not otherwise stated. All chemical shifts were referenced with respect to the H_2O signal at 4.77 ppm (pH 6.0, 25 °C) relative to DSS, using the $^1H/X$ frequency ratios of the zero point as described.[57]

For sequential backbone assignment of apo-CopK, three 2D-projection NMR experiments, 2D-HNCA, 2D-HN(CO)CA and 2D-HNCO, were recorded for the assignment of CO, $C^{\alpha}(i)$ and $C^{\alpha}(i-1)$ resonances.[58] The 2D approach was not successful for C^{β} assignment due to low sensitivity and signal overlaps. Therefore, a standard HNCACB experiment was acquired to complete the backbone assignment. Aliphatic carbon and proton sidechain resonances were assigned using three triple-resonance experiments (H(C)CONH-total correlated spectroscopy (TOCSY), (H)CCONH-TOCSY and HCCH-TOCSY). Aromatic proton resonance assignments were obtained from two 2D NOESY experiments acquired in H_2O and ^2H_2O with unlabeled protein dissolved in 50 mM potassium phosphate buffer, pH 6.0. Cu(I)-CopK backbone assignment was performed using a set of standard 3D experiments (HNCO, HNCACB, HN(CO)CACB, HNCA). An additional (H)CCONH-TOCSY experiment was acquired to verify the backbone assignment. Standard pulse sequences were taken from the Varian Bio-pack.

NMR distance restraints were derived from 3D ^{15}N-edited NOESY-HSQC, 3D ^{13}C-edited NOESY-HSQC and 3D methyl selective NOESY-HSQC experiments,[59] as well as from the two 2D-NOESY experiments acquired in H_2O and ^2H_2O. The following NOE mixing times were used: 100 ms for ^{13}C-edited NOESY-HSQC; 120 ms for ^{15}N-edited NOESY-HSQC and 2D-NOESY experiments; and 160 ms for 3D methyl selective NOESY-HSQC.

RDCs were collected on a uniformly ^{13}C,^{15}N-labeled sample suspended in a liquid-crystalline medium consisting of a mixture of 5% pentaethyleneglycol monododecyl ether (C12E5) and hexanol at a molar ratio of 0.96.[30] $^1D_{NH}$ and $^1D_{C'C\alpha}$ couplings were obtained using 3D HNCO-type experiments,[60] and calculated from the difference between the splittings measured in the isotropic and in the anisotropic sample after fitting the peaks to a Gaussian lineshape. RDCs varied between 15.6 Hz and –8.3 Hz for $^1D_{NH}$ and between 3.46 Hz and –6.23 Hz for $^1D_{C'C\alpha}$ couplings. For the structure calculation, the $^1D_{C'C\alpha}$ couplings were scaled by a factor of 0.5 to take stronger sample alignment into account. The final error was estimated to 0.5 Hz for $^1D_{NH}$ and 0.25 Hz for $^1D_{C'C\alpha}$ couplings.

All NMR spectra were processed and analyzed using NMRPipe[61] and NMRView.[62,63]

Metal binding by NMR

Samples contained 0.4 mM of uniformly ^{15}N-labeled CopK protein in 50 mM ammonium acetate (pH 6.8) and one or two molar equivalents of Cu(II) or Cu(I). For the backbone assignment of Cu(I)-CopK, 450 μL of doubly labeled CopK was mixed with 1 mol. eq. of $Cu(II)Cl_2$ in the presence of 10 mM sodium ascorbate and 50 μL of ^2H_2O. The final protein concentration was 1 mM. For the determination of ^{15}N chemical shifts in the histidine imidazole rings, a modified SOFAST-HMQC experiment,[64] optimized for the detection of $^2J_{NH}$ couplings, was performed on 1.2 mM uniformly ^{15}N-labeled apo- and Cu(I)-CopK dissolved in ^2H_2O. In this experiment, the selective proton pulses were centered at 7.4 ppm with a bandwidth of 2.5 ppm, the ^{15}N carrier was set to 190 ppm and 1024 complex points were acquired in the indirect dimension to cover a ^{15}N spectral width of 12,800 Hz at a ^{15}N frequency of 81 MHz. The transfer delay was set to 25 ms. Two-dimensional HET-SOFAST experiments were acquired on 0.4 mM samples of apo- and 1Cu(I)-bound CopK with and without inversion of aliphatic proton resonances as described.[36] The HN-selective pulses were centered at 9 ppm. The λ_{NOE} values were calculated as the ratio of peak intensities (I_{sat}/I_{ref}) and averaged over all peaks.

^{15}N-relaxation experiments

R_1, $R_{1\rho}$, R_2 and {^1H}-^{15}N hetNOE relaxation experiments were acquired at 600 MHz using standard pulse sequences[65] on uniformly ^{15}N labeled apo-CopK at three different concentrations (1.5 mM, 1.3 mM and 0.3 mM). For Cu(I)-CopK, R_1, $R_{1\rho}$, R_2 relaxation rates were measured on a 0.6 mM uniformly ^{15}N labeled sample in the presence of one molar equivalent of Cu(I). During the R_1 relaxation delays, cross-correlated relaxation was suppressed by applying a 550 μs cosine-modulated 180° squared pulse every 5 ms with an excitation maximum of 2 kHz from the carrier. The transverse relaxation rates were calculated either from the R_2(CPMG) experiment or from $R_{1\rho}$ rate constants, using the relation:

$$R_{1\rho} = \cos^2(\theta)R_2 + \sin^2(\theta)R_1$$

with:

$$\theta = \tan^{-1}(2\pi\Delta\nu/\gamma_N B_1)$$

§ available at http://www.analyticalultracentrifugation.com

ǁ available at http://www.jphilo.mailway.com/download.htm

where $\Delta\nu$ is the ^{15}N resonance offset. The recycle delay was set to 3 s for the R_1, R_2, and the $R_{1\rho}$ experiments. The relaxation-caused magnetization decay was sampled at 10, 30, 60, 120, 180, 240, 300, 400, 600, 900 and 1100 ms for longitudinal and at 10, 30, 50, 70, 130, 170, 210 and 250 ms for transverse relaxation. The $\{^1H\}^{15}N$-hetNOE, recorded only on the 1.5 mM apo-CopK sample, was determined from two spectra with on and off resonance ^1H saturation and recorded in an interleaved manner. The saturation and the recycle delay were set to 3 s and 5 s, respectively. Peak intensities were measured using NMRView and relaxation rates were extracted using the program Curvefit¶ with a two-parameter single exponential and a Monte Carlo simulation for error estimation. The characteristics of the protein mobility were further analyzed using the Tensor2 program,[32] with the longitudinal and the $R_{1\rho}$-derived transverse relaxation rate constants as input data and a minimal error of 5%.

Amide H/D exchange

Amide H/D exchange rates were measured with the SOFAST real time 2D NMR approach.[35] A 300 μl sample of 1.5 mM CopK in 50 mM Mes buffer (pH 6.0) was concentrated to 60 μl in a SpeedVac device. This solution was injected into 350 μL of ^2H_2O inside the spectrometer using a rapid injection device. The final protein concentration was 1.1 mM and the pH was 6.5 (corrected for the glass electrode isotope effect). The decay of crosspeaks was followed at 297 K with a series of 2D ^1H-^{15}N SOFAST HMQC spectra with a duration of 6.7 s for each experiment, allowing quantification of exchange rates up to 0.1 s^{-1}. The peak intensities were fit to a three-parameter monoexponential decay function and error bars were obtained from Monte Carlo analysis based on twice the baseline noise.

The data were interpreted with the EX2 model,[34] where the thermodynamic equilibrium constant K_{op} is given as the ratio of observed and intrinsic exchange rates. The intrinsic rates were determined as described, taking into account explicitly the isotopic effects of the $H_2O/^2H_2O$-mixture used here.[66,67]

NOE assignment and structure calculation of apo-CopK

The program ATNOS/CANDID[28,29] interfaced to CNS[68] was used for automatic peak picking and NOE assignment, together with a list of manually assigned long-range NOEs involving methyl and aromatic side-chain protons. The resulting distance restraints were used as input for Aria1.2,[69] together with Talos restraints for the secondary structure elements.[70] Structure calculation was performed with protocols described for the constitution of the RECOORD database.[71] In the final calculation, the converged structures from the precedent Aria1.2 run were refined with RDC constraints. The axial (D) and rhombic (r) components of the alignment tensor were determined using the program MODULE[31] with:

$$D = (\mu_0/16\pi^3)h\gamma_i\gamma_j(r_{ij})^{-3}Aa$$

$$r = Ar/Aa$$

The 50 structures with the lowest total energy were selected and further refined in explicit water. From the resulting ensemble of 1000 structures, the 20 structures with the lowest total energy were selected and form the representative structural ensemble.

Protein Data Bank accession code

Chemical shift assignments and molecular coordinates have been deposited with the BioMagResBank[a] under the accession number 15655 and the Protein Data Bank[b] under the accession number 2K0Q, respectively.

Acknowledgements

We are very grateful to Isabel Ayala for protein purification, and to Klaartje Houbens for her help with the setup and interpretation of the relaxation experiments and the resulting stimulating discussions. Aline Appourchaux, Eva Rosenbaum, and Christine Ebel are acknowledged for the analytical ultracentrifugation experiments. R.W is a Research Associate of FNRS. This work was supported by the Commissariat à l'Energie Atomique, the Centre National de la Recherche Scientifique and the Université Joseph Fourier.

Supplementary Data

Supplementary data associated with this article can be found, in the online version, at doi:10.1016/j.jmb.2008.05.017

References

1. Pena, M. M., Lee, J. & Thiele, D. J. (1999). A delicate balance: homeostatic control of copper uptake and distribution. *J. Nutr.* **129**, 1251–1260.
2. Puig, S. & Thiele, D. J. (2002). Molecular mechanisms of copper uptake and distribution. *Curr. Opin. Chem. Biol.* **6**, 171–180.
3. Lippard, S. J. (1999). Free copper ions in the cell? *Science*, **284**, 748–749.
4. La Fontaine, S. & Mercer, J. F. (2007). Trafficking of the copper-ATPases, ATP7A and ATP7B: role in copper homeostasis. *Arch. Biochem. Biophys.* **463**, 149–167.
5. Gaggelli, E., Kozlowski, H., Valensin, D. & Valensin, G. (2006). Copper homeostasis and neurodegenerative disorders (Alzheimer's, prion, and Parkinson's diseases and amyotrophic lateral sclerosis). *Chem. Rev.* **106**, 1995–2044.
6. Nies, D. H. (1999). Microbial heavy-metal resistance. *Applied Microbiology*, **51**, 730–750.
7. Brown, N. L., Rouch, D. A. & Lee, B. T. (1992). Copper resistance determinants in bacteria. *Plasmid*, **27**, 41–51.
8. Brown, N. L., Barrett, S. R., Camakaris, J., Lee, B. T. & Rouch, D. A. (1995). Molecular genetics and transport analysis of the copper-resistance determinant (pco) from *Escherichia coli* plasmid pRJ1004. *Mol. Microbiol.* **17**, 1153–1166.

¶ http://cpmcnet.columbia.edu/dept/gsas/biochem/labs/palmer/software/curvefit.html

[a] www.bmrb.wisc.edu
[b] www.pdb.org

9. Rensing, C. & Grass, G. (2003). *Escherichia coli* mechanisms of copper homeostasis in a changing environment. *FEMS Microbiol. Rev.* **27**, 197–213.
10. Lee, S. M., Grass, G., Rensing, C., Barrett, S. R., Yates, C. J., Stoyanov, J. V. & Brown, N. L. (2002). The Pco proteins are involved in periplasmic copper handling in *Escherichia coli*. *Biochem. Biophys. Res. Commun.* **295**, 616–620.
11. Chen, Y. T., Chang, H. Y., Lai, Y. C., Pan, C. C., Tsai, S. F. & Peng, H. L. (2004). Sequencing and analysis of the large virulence plasmid pLVPK of *Klebsiella pneumoniae* CG43. *Gene*, **337**, 189–198.
12. Adaikkalam, V. & Swarup, S. (2005). Characterization of copABCD operon from a copper-sensitive *Pseudomonas putida* strain. *Can. J. Microbiol.* **51**, 209–216.
13. Solioz, M. & Stoyanov, J. V. (2003). Copper homeostasis in *Enterococcus hirae*. *FEMS Microbiol. Rev.* **27**, 183–195.
14. Mills, S. D., Lim, C. K. & Cooksey, D. A. (1994). Purification and characterization of CopR, a transcriptional activator protein that binds to a conserved domain (cop box) in copper-inducible promoters of *Pseudomonas syringae*. *Mol. Gen. Genet.* **244**, 341–351.
15. Vandamme, P. & Coenye, T. (2004). Taxonomy of the genus *Cupriavidus*: a tale of lost and found. *Int. J. Syst. Evol. Microbiol.* **54**, 2285–2289.
16. Brim, H., Heyndrickx, M., de Vos, P., Wilmotte, A., Springael, D., Schlegel, H. G. & Mergeay, M. (1999). Amplified rDNA restriction analysis and further genotypic characterisation of metal-resistant soil bacteria and related facultative hydrogenotrophs. *Syst. Appl. Microbiol.* **22**, 258–268.
17. Goris, J., De Vos, P., Coenye, T., Hoste, B., Janssens, D., Brim, H. *et al.* (2001). Classification of metal-resistant bacteria from industrial biotopes as *Ralstonia campinensis* sp. nov., *Ralstonia metallidurans* sp. nov. and *Ralstonia basilensis* Steinle *et al*. 1998 emend. *Int. J. Syst. Evol. Microbiol.* **51**, 1773–1782.
18. Mergeay, M. (2000). Bacteria adapted to industrial biotopes: the metal-resistant *Ralstonia*. In *Bacterial Stress Responses* (Storz, G. & Hengge-Aronis, R., eds), pp. 403–414, ASM Press, Washington, DC.
19. Nies, D. H., Rehbein, G., Hoffmann, T., Baumann, C. & Grosse, C. (2006). Paralogs of genes encoding metal resistance proteins in *Cupriavidus metallidurans* strain CH34. *J. Mol. Microbiol. Biotechnol.* **11**, 82–93.
20. Mergeay, M., Monchy, S., Vallaeys, T., Auquier, V., Benotmane, A., Bertin, P. *et al.* (2003). *Ralstonia metallidurans*, a bacterium specifically adapted to toxic metals: towards a catalogue of metal-responsive genes. *FEMS Microbiol. Rev.* **27**, 385–410.
21. Borremans, B., Hobman, J. L., Provoost, A., Brown, N. L. & van Der Lelie, D. (2001). Cloning and functional analysis of the pbr lead resistance determinant of *Ralstonia metallidurans* CH34. *J. Bacteriol.* **183**, 5651–5658.
22. Monchy, S., Benotmane, M. A., Janssen, P., Vallaeys, T., Taghavi, S., van der Lelie, D. & Mergeay, M. (2007). Plasmids pMOL28 and pMOL30 of *Cupriavidus metallidurans* are specialized in the maximal viable response to heavy metals. *J. Bacteriol.* **189**, 7417–7425.
23. Monchy, S., Benotmane, M. A., Wattiez, R., van Aelst, S., Auquier, V., Borremans, B. *et al.* (2006). Transcriptomic and proteomic analyses of the pMOL30-encoded copper resistance in *Cupriavidus metallidurans* strain CH34. *Microbiology*, **152**, 1765–1776.
24. Monchy, S., Vallaeys, T., Bossus, A. & Mergeay, M. (2006). Transcriptomic analysis of the *Ralstonia metallidurans* CH34 genes encoding for P-ATPases. *Int. J. Environ. Anal. Chem.* **86**, 677–692.
25. Tricot, C., van Aelst, S., Wattiez, R., Mergeay, M., Stalon, V. & Wouters, J. (2005). Overexpression, purification, crystallization and crystallographic analysis of CopK of *Cupriavidus metallidurans*. *Acta Crystallogr. F*, **61**, 825–827.
26. Jiang, J., Nadas, I. A., Kim, M. A. & Franz, K. J. (2005). A Mets motif peptide found in copper transport proteins selectively binds Cu(I) with methionine-only coordination. *Inorg. Chem.* **44**, 9787–9794.
27. Urvoas, A., Amekraz, B., Moulin, C., Le Clainche, L., Stocklin, R. & Moutiez, M. (2003). Analysis of the metal-binding selectivity of the metallochaperone CopZ from *Enterococcus hirae* by electrospray ionization mass spectrometry. *Rapid Commun. Mass Spectrom.* **17**, 1889–1896.
28. Herrmann, T., Guntert, P. & Wuthrich, K. (2002). Protein NMR structure determination with automated NOE-identification in the NOESY spectra using the new software ATNOS. *J. Biomol. NMR*, **24**, 171–189.
29. Herrmann, T., Guntert, P. & Wuthrich, K. (2002). Protein NMR structure determination with automated NOE assignment using the new software CANDID and the torsion angle dynamics algorithm DYANA. *J. Mol. Biol.* **319**, 209–227.
30. Rückert, M. & Otting, G. (2000). Alignment of biological macromolecules in novel nonionic liquid crystalline media for NMR experiments. *J. Am. Chem. Soc.* **122**, 7793–7797.
31. Dosset, P., Hus, J. C., Marion, D. & Blackledge, M. (2001). A novel interactive tool for rigid-body modeling of multi-domain macromolecules using residual dipolar couplings. *J. Biomol. NMR*, **20**, 223–231.
32. Dosset, P., Hus, J. C., Blackledge, M. & Marion, D. (2000). Efficient analysis of macromolecular rotational diffusion from heteronuclear relaxation data. *J. Biomol. NMR*, **16**, 23–28.
33. Garcia de la Torre, J., Huertas, M. L. & Carrasco, B. (2000). HYDRONMR: prediction of NMR relaxation of globular proteins from atomic-level structures and hydrodynamic calculations. *J. Magn. Reson.* **147**, 138–146.
34. Dempsey, C. (2001). Hydrogen exchange in peptides and proteins using NMR spectroscopy. *Prog. Nucl. Magn. Res. Spectrosc.* **39**, 135–170.
35. Schanda, P., Forge, V. & Brutscher, B. (2007). Protein folding and unfolding studied at atomic resolution by fast two-dimensional NMR spectroscopy. *Proc. Natl Acad. Sci. USA*, **104**, 11257–11262.
36. Schanda, P., Forge, V. & Brutscher, B. (2006). HET-SOFAST NMR for fast detection of structural compactness and heterogeneity along polypeptide chains. *Magn. Reson. Chem.* **44**, S177–S184.
37. Wishart, D. S. & Sykes, B. D. (1994). The ^{13}C chemical-shift index: a simple method for the identification of protein secondary structure using ^{13}C chemical-shift data. *J. Biomol. NMR*, **4**, 171–180.
38. Pelton, J. G., Torchia, D. A., Meadow, N. D. & Roseman, S. (1993). Tautomeric states of the active-site histidines of phosphorylated and unphosphorylated III^{Glc}, a signal-transducing protein from *Escherichia coli*, using two-dimensional heteronuclear NMR techniques. *Protein Sci.* **2**, 543–558.
39. Banci, L., Bertini, I., Ciofi-Baffoni, S., Su, X. C., Borrelly, G. P. & Robinson, N. J. (2004). Solution structures of a cyanobacterial metallochaperone: insight into an atypical copper-binding motif. *J. Biol. Chem.* **279**, 27502–27510.
40. Peariso, K., Huffman, D. L., Penner-Hahn, J. E. & O'Halloran, T. V. (2003). The PcoC copper resistance

protein coordinates Cu(I) *via* novel S-methionine interactions. *J. Am. Chem. Soc.* **125**, 342–343.
41. Zhang, L., Koay, M., Maher, M. J., Xiao, Z. & Wedd, A. G. (2006). Intermolecular transfer of copper ions from the CopC protein of *Pseudomonas syringae*. Crystal structures of fully loaded Cu(I)Cu(II) forms. *J. Am. Chem. Soc.* **128**, 5834–5850.
42. Loftin, I. R., Franke, S., Roberts, S. A., Weichsel, A., Heroux, A., Montfort, W. R. *et al.* (2005). A novel copper-binding fold for the periplasmic copper resistance protein CusF. *Biochemistry*, **44**, 10533–10540.
43. Arnesano, F., Banci, L., Bertini, I., Ciofi-Baffoni, S., Molteni, E., Huffman, D. L. & O'Halloran, T. V. (2002). Metallochaperones and metal-transporting ATPases: a comparative analysis of sequences and structures. *Genome Res.* **12**, 255–271.
44. Arnesano, F., Banci, L., Bertini, I. & Thompsett, A. R. (2002). Solution structure of CopC: a cupredoxin-like protein involved in copper homeostasis. *Structure*, **10**, 1337–1347.
45. Arnesano, F., Banci, L., Bertini, I., Mangani, S. & Thompsett, A. R. (2003). A redox switch in CopC: an intriguing copper trafficking protein that binds copper (I) and copper(II) at different sites. *Proc. Natl Acad. Sci. USA*, **100**, 3814–3819.
46. Wernimont, A. K., Huffman, D. L., Finney, L. A., Demeler, B., O'Halloran, T. V. & Rosenzweig, A. C. (2003). Crystal structure and dimerization equilibria of PcoC, a methionine-rich copper resistance protein from *Escherichia coli*. *J. Biol. Inorg. Chem.* **8**, 185–194.
47. Banci, L., Bertini, I., Ciofi-Baffoni, S., Katsari, E., Katsaros, N., Kubicek, K. & Mangani, S. (2005). A copper(I) protein possibly involved in the assembly of Cu_A center of bacterial cytochrome *c* oxidase. *Proc. Natl Acad. Sci. USA*, **102**, 3994–3999.
48. Djoko, K. Y., Xiao, Z., Huffman, D. L. & Wedd, A. G. (2007). Conserved mechanism of copper binding and transfer. A comparison of the copper-resistance proteins PcoC from *Escherichia coli* and CopC from *Pseudomonas syringae*. *Inorg. Chem.* **46**, 4560–4568.
49. Loftin, I. R., Franke, S., Blackburn, N. J. & McEvoy, M. M. (2007). Unusual Cu(I)/Ag(I) coordination of *Escherichia coli* CusF as revealed by atomic resolution crystallography and X-ray absorption spectroscopy. *Protein Sci.* **16**, 2287–2293.
50. Xue, Y., Davis, A. V., Balakrishnan, G., Stasser, J. P., Staehlin, B. M., Focia, P. *et al.* (2008). Cu(I) recognition *via* cation-π and methionine interactions in CusF. *Nature Chem. Biol.* **4**, 107–109.
51. Kittleson, J. T., Loftin, I. R., Hausrath, A. C., Engelhardt, K. P., Rensing, C. & McEvoy, M. M. (2006). Periplasmic metal-resistance protein CusF exhibits high affinity and specificity for both Cu^I and Ag^I. *Biochemistry*, **45**, 11096–11102.
52. Zoropogui, A., Gambarelli, S. & Coves, J. (2008). CzcE from *Cupriavidus metallidurans* CH34 is a copper-binding protein. *Biochem. Biophys. Res. Commun.* **365**, 735–739.
53. Sendra, V., Cannella, D., Bersch, B., Fieschi, F., Menage, S., Lascoux, D. & Coves, J. (2006). CopH from *Cupriavidus metallidurans* CH34. A novel periplasmic copper-binding protein. *Biochemistry*, **45**, 5557–5566.
54. Holm, L. & Sander, C. (1993). Protein structure comparison by alignment of distance matrices. *J. Mol. Biol.* **233**, 123–138.
55. Jansson, M., Li, Y. C., Jendeberg, L., Anderson, S., Montelione, B. T. & Nilsson, B. (1996). High-level production of uniformly ^{15}N- and ^{13}C-enriched fusion proteins in *Escherichia coli*. *J. Biomol. NMR*, **7**, 131–141.
56. Schuck, P. (2000). Size-distribution analysis of macromolecules by sedimentation velocity ultracentrifugation and lamm equation modeling. *Biophys. J.* **78**, 1606–1619.
57. Markley, J. L., Bax, A., Arata, Y., Hilbers, C. W., Kaptein, R., Sykes, B. D. *et al.* (1998). Recommendations for the presentation of NMR structures of proteins and nucleic acids. IUPAC-IUBMB-IUPAB Inter-Union Task Group on the Standardization of Data Bases of Protein and Nucleic Acid Structures Determined by NMR Spectroscopy. *J. Biomol. NMR*, **12**, 1–23.
58. Bersch, B., Rossy, E., Coves, J. & Brutscher, B. (2003). Optimized set of two-dimensional experiments for fast sequential assignment, secondary structure determination, and backbone fold validation of $^{13}C/^{15}N$-labelled proteins. *J. Biomol. NMR*, **27**, 57–67.
59. Van Melckebeke, H., Simorre, J. P. & Brutscher, B. (2004). Amino acid-type edited NMR experiments for methyl-methyl distance measurement in ^{13}C-labeled proteins. *J. Am. Chem. Soc.* **126**, 9584–9591.
60. Brutscher, B. (2001). Accurate measurement of small spin-spin couplings in partially aligned molecules using a novel J-mismatch compensated spin-state-selection filter. *J. Magn. Reson.* **151**, 332–338.
61. Delaglio, F., Grzesiek, S., Vuister, G. W., Zhu, G., Pfeifer, J. & Bax, A. (1995). NMRPipe: a multidimensional spectral processing system based on UNIX pipes. *J. Biomol. NMR*, **6**, 277–293.
62. Johnson, B. A. & Blevins, R. A. (1994). NMR View: a computer program for the visualization and analysis of NMR data. *J. Biomol. NMR*, **4**, 603–614.
63. Johnson, B. A. (2004). Using NMRView to visualize and analyze the NMR spectra of macromolecules. *Methods Mol. Biol.* **278**, 313–352.
64. Schanda, P., Kupce, E. & Brutscher, B. (2005). SOFAST-HMQC experiments for recording two-dimensional heteronuclear correlation spectra of proteins within a few seconds. *J. Biomol. NMR*, **33**, 199–211.
65. Farrow, N. A., Muhandiram, R., Singer, A. U., Pascal, S. M., Kay, C. M., Gish, G. *et al.* (1994). Backbone dynamics of a free and phosphopeptide-complexed Src homology 2 domain studied by ^{15}N NMR relaxation. *Biochemistry*, **33**, 5984–6003.
66. Bai, Y., Milne, J. S., Mayne, L. & Englander, S. W. (1993). Primary structure effects on peptide group hydrogen exchange. *Proteins: Struct. Funct. Genet.* **17**, 75–86.
67. Connelly, G. P., Bai, Y., Jeng, M. F. & Englander, S. W. (1993). Isotope effects in peptide group hydrogen exchange. *Proteins: Struct. Funct. Genet.* **17**, 87–92.
68. Brunger, A. T., Adams, P. D., Clore, G. M., DeLano, W. L., Gros, P., Grosse-Kunstleve, R. W. *et al.* (1998). Crystallography and NMR system: A new software suite for macromolecular structure determination. *Acta Crystallogr. D*, **54**, 905–921.
69. Nilges, M., Macias, M. J., O'Donoghue, S. I. & Oschkinat, H. (1997). Automated NOESY interpretation with ambiguous distance restraints: the refined NMR solution structure of the pleckstrin homology domain from beta-spectrin. *J. Mol. Biol.* **269**, 408–422.
70. Cornilescu, G., Delaglio, F. & Bax, A. (1999). Protein backbone angle restraints from searching a database for chemical shift and sequence homology. *J. Biomol. NMR*, **13**, 289–302.
71. Nederveen, A. J., Doreleijers, J. F., Vranken, W., Miller, Z., Spronk, C. A., Nabuurs, S. B. *et al.* (2005). RECOORD: a recalculated coordinate database of 500+ proteins from the PDB using restraints from the BioMagResBank. *Proteins: Struct. Funct. Genet.* **59**, 662–672.